



# An integrated simulation framework for the prevention and mitigation of pandemics caused by airborne pathogens

Christos Chondros<sup>1</sup> · Stavros D. Nikolopoulos<sup>1</sup> · Iosif Polenakis<sup>1</sup>

Received: 10 November 2021 / Revised: 24 September 2022 / Accepted: 24 September 2022  
© The Author(s), under exclusive licence to Springer-Verlag GmbH Austria, part of Springer Nature 2022

## Abstract

In this work, we developed an integrated simulation framework for pandemic prevention and mitigation of pandemics caused by airborne pathogens, incorporating three sub-models, namely the spatial model, the mobility model, and the propagation model, to create a realistic simulation environment for the evaluation of the effectiveness of different countermeasures on the epidemic dynamics. The spatial model converts images of real cities obtained from Google Maps into undirected weighted graphs that capture the spatial arrangement of the streets utilized next for the mobility of individuals. The mobility model implements a stochastic agent-based approach, developed to assign specific routes to individuals moving in the city, through the use of stochastic processes, utilizing the weights of the underlying graph to deploy shortest path algorithms. The propagation model implements both the epidemiological model and the physical substance of the transmission of an airborne pathogen (in our approach, we investigate the transmission parameters of SARS-CoV-2). The deployment of a set of countermeasures was investigated in reducing the spread of the pathogen, where, through a series of repetitive simulation experiments, we evaluated the effectiveness of each countermeasure in pandemic prevention.

**Keywords** Simulation · Epidemic control · Airborne pathogens · Algorithms · Graph theory

## 1 Introduction

The recent outbreak of a disease caused by an airborne transmitted pathogen brought to forefront the vital need for more extensive research over the aspect of technologies that could efficiently and effectively provide solutions to such needs. In this work, we study the parameters that contribute to the spread of airborne pathogens among the individuals of a population and propose an integrated simulation framework that prevents the development of an epidemic to a pandemic, considering mostly the reproduction and transmission parameters of the airborne virus SARS-CoV-2. Next, we discuss the basic properties of epidemiology and

pandemic prevention, present the related work, and provide a brief introduction about the approach proposed in this work.

### 1.1 Preventing pandemics

In 2019, a new virus appeared, as a strain of Coronaviridae emerging as a mutation of the known SARS virus, namely the SARS-CoV-2 that caused the so-called COVID-19 disease that finally developed to a pandemic. As described by (Cirrincione et al. 2020), several countermeasures there should be applied as soon as possible to avoid the transmission of the new coronavirus. Preventing the spread of a disease in order not to be developed in a level such that the vast majority of the population to get infected, i.e., a pandemic occurs, several countermeasures have to be taken. (Manika and Golden 2011) investigating the influenza pandemic caused by H1N1 conclude that the prevention of a pandemic could be more effective by mitigating its effects.

Several pathogens have been transmitted from animals to humans by several pathways (Loh et al. 2015) and by mutating themselves spread among individuals evolved to pandemics. As described by (Hughes et al. 2010), the interface between humans and animals is of

✉ Stavros D. Nikolopoulos  
stavros@cs.uoi.gr

Christos Chondros  
cs02573@uoi.gr

Iosif Polenakis  
ipolenak@cs.uoi.gr

<sup>1</sup> Department of Computer Science and Engineering,  
University of Ioannina, 45100 Ioannina, Greece

major importance in the process, suggesting, hence, a key point in the emerging of pandemics as their investigation may result to the development of prevention strategies. (Morse et al. 2012) throughout their investigation over the emerging pathogens regarding their origination, the interface of transmission to humans, etc. conclude that the deployment of mathematical modeling and information technologies can provide a crucial effort in the recognition of new pathogens and provide to a further extent new risk assessments. (Jung et al. 2009) investigate the case study of influenza pandemic and the role of time-dependent prevention strategies, highlighting the major importance of quarantine as a countermeasure for pandemic prevention. Regarding the original strain of SARS-CoV-2, (Karita et al. 2022) provide a thorough study over the trajectory of viral load among persons with incident SARS-CoV-2 concluding that the rapid viral replication indicates the very narrow period for effective antiviral intervention. Finally, (Stawicki et al. 2020) emphasize on the integration of the data available for the COVID-19 pandemic and how they could be deployed to strength the pandemic readiness highlighting some of the observed gaps in preparedness based on the collected data.

## 1.2 Related work

Epidemic modeling and mitigation of pandemics have been extensively studied through the literature, especially during the latest years where the outbreak of SARS-Cov-2 has brought to foreground the necessity for developing countermeasures able to suppress the spread of a pathogen effectively. (Obadia et al. 2012) review the methods for the estimation of transmissibility parameters during outbreaks and implement five of them as a toolbox of sensitivity analysis tools to estimate the serial interval distribution and reproduction numbers in epidemics, reporting a numerical comparison to explore the sensitivity of estimates among them. (Britton 2010) provided a survey over the stochastic epidemic models, by defining the properties of the deterministic and the stochastic model and how they can be used to meet several epidemiological conditions, describing finally a model for endemic disease. (Keeling and Eames 2005) provide a review over the basis of epidemiological and network theory suggesting finally how these research fields can be combined to reveal insights of disease dynamics providing, hence, a more effective disease control. Next, we present the related approaches proposed through the literature during the latest years. We distinguish three categories, namely the related works concerning the modeling of epidemics, the mitigation of epidemics, and the investigation of the factors that affect the spread of pathogens, respectively.

### 1.2.1 Epidemic modeling

(Cliff et al. 2018) presented an agent-based modeling framework for studying influenza, analyzing spatiotemporal spread. Like the approach proposed in this work, mobility patterns were gathered from national data source to trace the spread dynamics. Their experimental study included quantitative and qualitative of the spatiotemporal profiles. (Modi et al. 2021) utilized online data in order to estimate the progression of COVID-19 spread utilizing the SEIR epidemic compartmental model, including the states (Susceptible–Exposed–Infected–Recovered), over various values of  $R_0$ . (Duan et al. 2015) Duan investigate the three major types of epidemic modeling, namely the mathematical, the complex network and the agent-based models, providing a comprehensive review over the exhibited main principles, and the advantages and disadvantages they exhibit over they application. (Valdano et al. 2018) proposed a framework for the computation of epidemic threshold, providing a coherent connection between discrete and continuous time representations applicable to realistic scenarios to investigate the biasing of outbreak results throughout the conditions of continuous-time evolving networks. (Liu et al. 2018) study analytically and numerically the epidemic spreading threshold, facing the multiplexity and the temporal nature of connectivity patterns exhibited both in time-varying networks, proposing a time-varying model of multiplex networks upon the SIS epidemic model.

### 1.2.2 Epidemic control

(Kovacevic et al. 2020) propose a distributed (continuous-time) epidemic model to describe the dynamics of an epidemic taking into account the social distancing, utilizing the statistical information rather the traditional state transition utilized in the most compartmental models. A novelty of the proposed approach arises from its ability to fit the case study of the COVID-19 disease where the incubation period lasts longer than usual. The proposed model additionally allows the analysis of combined intervention strategies with less adaption in the main equations. (Currie et al. 2020) describe the whole current status over the value of simulation and modeling against the spread SARS-CoV-2 virus and the corresponding COVID-19, discussing how such approaches could provide significant help in decision making and to a further extent to contribute in pandemic prevention. (Hufnagel et al. 2004) investigate the control of epidemic in worldwide level. Their proposed stochastic model is consisted by two sub-model referencing firstly the infection dynamics and further the transmission dynamics in global terms. (Cuevas-Maraver et al. 2021) explore the impact of lock-down measures on single-age and two-age structured epidemic model for the COVID-19 outbreak,

having as a case study the country of Mexico, utilizing an extension of the SEIR epidemic model that includes a pre-symptomatic stage, during which a person experiences no symptoms, but is nevertheless infectious.

### 1.2.3 Factor investigation

(Kevrekidis et al. 2021) investigate the spatial modeling of the SARS-CoV-2 spread over Greece and Andalusia emphasizing in the incubation period regarding the effect it causes in the spread by the asymptomatic population. (Bertacchini et al. 2020) focus on characteristics of the SAR-CoV-2 propagation concerning mostly the temporal aspect of the spread. Throughout their investigation and analysis there has been shown that the complex behavior exhibited over COVID-19 disease results from spatiotemporal pandemic dynamics, while several valuable clues about the spread, that potential lead to the development of countermeasures, are revealed over the analysis of the context over which SARS-CoV-2 is developing. (Barmak et al. 2016) investigate the effect of the mobility of individuals on the pandemic spread focusing on the case study of dengue. In particular, through a stochastic model concerning the dynamics of the infected mosquitoes and humans, they investigated how the variations in mobility patterns affect most the dynamics of the epidemic spread.

Next, there are presented related approaches developed over the field of epidemic modeling that investigate the effect of the underlying time-varying contact networks among the individuals. (Masuda and Holme 2013) discuss how temporal contact networks contribute to the prediction and control of epidemic spread reviewing the results achieved from various methods over network epidemiology that utilize temporal network data. (Nadini et al. 2018) utilize time-varying networks deploying the SIR and SIS epidemic compartmental models, including the states (Susceptible–Infected–Recovered) and (Susceptible–Infected–Susceptible), respectively, to investigate the effect of temporal connectivity on epidemic spread. Their theory is confirmed over a series of experimental simulations utilizing synthetic or real modular and temporal network graphs. (Tizzani et al. 2018) utilizing the SIS and SIR epidemic models analyze the effect caused on the spread dynamics on networks by the time-varying topology of them and the memory effects in the pattern of interactions among individuals. (Becker and Grenfell 2017) utilize the tsIR alongside the time-series Susceptible–Infected–Recovered model inferring incidence data, to analyze data that depict time-series of diseases.

Next, there are presented related approaches developed over the field of simulation by the aspect of individual contact in terms of the underlying physics that guide the spread of airborne viruses concerning the infected respiratory droplets emitted by infected hosts. (Nicas et al. 2005) investigated

the risk of airborne infection causes by the emission of respirable pathogens focusing on predicting the infection risk over factors that include mostly the airborne concentration of pathogens carried on particles as also the volume of particles themselves. (Stilianakis and Drossinos 2010) propose an epidemiological model of transmission dynamics incorporating the dynamics of inhalable respiratory droplets, to assess the relevance the diameter of inhalable respiratory droplets to the infectious process, while (Drossinos and Stilianakis 2020) they present the importance behind the physics of airborne pathogen transmission as droplets are transmitted by the turbulent air-flow generated by a violent expiratory event. (Wei and Li 2016) investigated the effect of droplets on airborne spread and how this procedure is affected itself by human interaction such door opening or walking affecting consequently the spread of pathogens.

## 1.3 Our approach

Through the recent outbreak of SARS-Cov-2 pandemic COVID-19, several studies and research have been oriented on the defense line against pandemic mitigation. Encountering several infection cases, from which a significant amount results to ICU and a percentage of them do not survive, our research approach consists another effort to deploy computer science over the sector of public health, and to a further extent to mitigate the viral spread that could be potentially evolved to a pandemic. In this work, we study the propagation of airborne viruses and provide a method to model their spread to deploy graph-based methods preventing the extension of the spread to a pandemic. More precisely, we design, propose and develop three modeling components that integrate finally a simulation framework that examines the effect of the deployed countermeasures to prevent, or mitigate, a pandemic. In particular, in this work, the propagation of SARS-CoV-2 virus that causes the COVID-19 disease is investigated as a case study, and by modeling the context under which such a virus may spread, we deploy several countermeasures where after a series of simulation experiments utilizing the proposed framework valuable information is revealed about specific insights of the pandemic.

The integrated simulation framework (Algorithms Engineering Laboratory 2022) developed for the study of the spread of airborne viruses, (with respect, but not limited, to the dynamics of SARS-CoV-2 spread), deploys three sub-models, namely the spatial model, the mobility model, and the propagation model, responsible for the simulation of the area the population is moving and transmits the virus, the simulation of the mobility patterns followed by the members of a population inside a specific area, and the simulation of the dynamics and the context under which the simulated airborne virus is transmitted among the population, respectively. Having developed the integrated framework for the

provision of an as realistic as possible environment for the spread of an airborne virus, several countermeasures, e.g., lock-down measures that incorporate the density reduction of the population, an efficient contact tracing application that incorporates the utilization of short-range communications (i.e., Bluetooth) to track nearby contacts, as also combinations of the aforementioned countermeasures are deployed and experimentally examined to decide their effectiveness against a pandemic spread and to a further extent to pandemic prevention. Finally, besides the proposed countermeasures investigated for pandemic prevention through the utilization of the proposed simulation framework, the most important factor that affect most the spread were extensively examined throughout this research study, including the effect of response time in the deployment of a countermeasure, where through the provided experimental series there has been proven that, beyond prevention measures, the effect of early warning in terms of small response time in the deployment of a counter measure is crucial to mitigate or prevent the pandemic, while even for effective countermeasures if their deployment is delayed it may cause the spread to evolve to a pandemic.

#### 1.4 Contribution

Throughout this work, there has been conducted a research about the epidemiological status of the airborne virus spread regarding the dynamics of a potential pandemic and how the investigated countermeasures could affect the virus spread by preventing finally the pandemic. The main contribution of this work is the development of the integrated simulation framework that deploys a hybrid simulation model representing a complex system behavior, incorporating three sub-models, namely the spatial model, the mobility model and the propagation model. The proposed integrated simulation framework approaches in a very detailed way the simultaneous and precise modeling of several factors that affect the spread, ranging from the movements of individuals and the capturing of social patterns to the modeling of the evolution of the viral load inside an infected host that affects the pathogen's spread. Furthermore, the integrated simulation framework proposed in this work is fully parametric and can be modified to adapt to any simulation settings required for the modeling of any disease caused by airborne pathogens. In particular, the proposed model, incorporated by the integrated simulation framework developed for this study, is designed in that way as to support the tuning of several settings and parameters and adapt to any pathogen transmission properties to simulate its epidemic dynamics, allowing modifications that could be required for the underlying spatial, mobility or propagation models. Moreover, the proposed framework is able to incorporate, by the embedding various external algorithms, the implementation of several

countermeasures to study their effect on the behavior of a pandemic. Finally, a very valuable information that potentially could be of vital importance, is the results exhibited by the conducted investigation over the series of Monte Carlo experiments over the proposed countermeasures, regarding their effect on death rates in terms of numbers of patients that given a standard set of ICU positions is able to avoid potential deaths of patients that could not survive if their number exceeds the capacity of ICU positions.

## 2 The proposed model

In this section, we present the proposed integrated simulation model for the prevention and mitigation of pandemics. In particular, we discuss its basic components and present extensively the incorporated models, namely, the spatial model, the mobility model and the propagation model.

### 2.1 Model overview

The proposed model for pandemic prevention and epidemic mitigation is based upon three sub-models incorporated to develop an integrated framework for the simulation of the spread of an airborne pathogen among individuals that are moving inside a specific area of a city (Chondros et al. 2021). The proposed framework is consisted namely by the spatial model, the mobility model, and the propagation model. The `spatial model` simulates the structure of a given city regarding its topology with respect to the streets and the corresponding town's planning. The `mobility model` acts as an agent-based modeling approach for the simulation of the mobility patterns (i.e., the routes) followed by the individuals (in our case the citizens of a town) to move between specific points of the city. Finally, the `propagation model`, is responsible for the transmission of the airborne pathogen and to a further extent for the deployment of the underlying epidemic model alongside the airborne pathogen transmission specifications, in our case the ones exhibited by SARS-CoV-2 virus. A detailed overview of the proposed integrated simulation framework alongside its incorporated model components, i.e., the spatial, the mobility and the propagation models and the underlying procedures under each one, is depicted in Fig. 1.

### 2.2 Spatial model

Next, we present the deployment of the proposed spatial model incorporated by our integrated framework for pandemic prevention and epidemic mitigation. We first discuss the transformation of an image taken from Google Maps to an object that depicts the structure of a city, modeling among others the orientations exhibited by the city roads, the

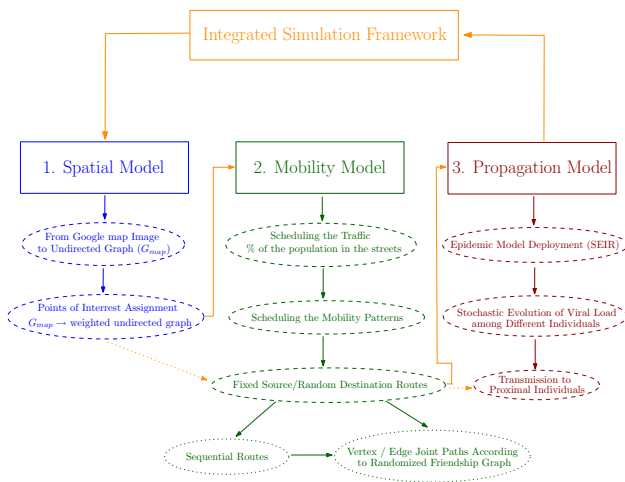


**Fig. 1** Architecture of the proposed integrated simulation framework for the prevention and mitigation of pandemics caused by airborne transmitted diseases

“points of interest” that attract the individuals’ routes, and next the construction of the underlying undirected weighted graph utilized for the construction of the paths in the corresponding routes.

**2.2.1 From Google Maps images to undirected graphs**

In our approach, we utilize and extend the approach presented initially in (Nikolopoulos and Polenakis 2016) and (Nikolopoulos and Polenakis 2017) deploying the simulation of the underlying texture that represents the area within which the individuals are moving, by utilizing real images of cities obtained from Google Maps and, after several image processing procedures, transforming them into graph objects handled by our model to define routes and paths following the street’s orientation and the topology of the town’s planning of the city under consideration. More precisely, given a image file from Google Maps (e.g., in

.jpeg format) we firstly transform it to gray-scale and then, applying a thresholding procedure, we transform it to a black-and-white image, where roads are presented by white color and buildings and obstacles are presented with black color. Finally, we edit the black-and-white image to indicate specific areas of the map, where they are located in the black-and-white image, that exhibit more congestion in terms of individual traffic, the so-called Points of Interest that we will discuss later. The purpose of this operation is a detailed graph-based representation of the image’s roads, that models the roads of the city, required for the simulation. At the end of the transformation, an undirected graph is constructed, whose vertex set corresponds to a square spot of the street (i.e., white-colored pixel of the image), while an edge belongs to the edge set of the graph if its corresponding end-points are neighboring square spots of the street based on their 7-neighborhood, where the 7-neighborhood of a cell, let  $(p, q)$ , consists of seven neighboring cells are from upper-left to lower-right:  $(p - 1, q - 1)$ ,  $(p - 1, q)$ ,  $(p, q + 1)$ ,  $(p, q - 1)$ ,  $(p, q + 1)$ ,  $(p + 1, q - 1)$ ,  $(p + 1, q)$ , and  $(p + 1, q + 1)$ .

The proposed model transforms any given image of any size into a graph alongside all the auxiliary information required. Our main goal is to create a graph whose vertex set corresponds to the streets from the given image taken from Google Maps, modeling the area in which the propagation is investigated. The whole procedure for transforming an image taken from Google Maps to its corresponding graph representation follows the next steps:

1. We first select the preferred area from Google Maps, see Fig. 2a, capturing the corresponding segment cropping it as an image, and finally omitting the irrelevant information, i.e., tags, names etc. Next, following the image processing procedure described above, we transform the initial image taken from Google Maps into a 2D matrix, with each particular cell containing three different values (i.e., the RGB color index of each pixel).



**Fig. 2** Example of the image transformation procedure

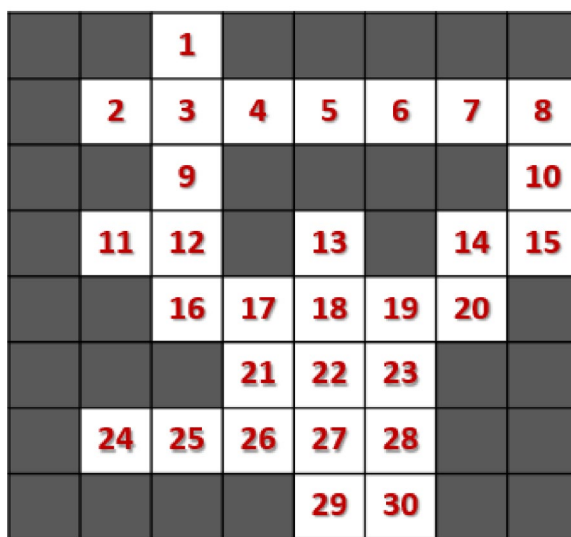
2. To distinguish the cells that correspond to streets and the cells that correspond to buildings, we first transform the initial image into a gray-scale image, casting the RGB index value of each cell into a single value that represents the intensity of gray color, and apply a thresholding procedure defined by specific image characteristics, see Fig. 2b.
3. In our approach we consider that the cell values of the matrix above the specified threshold value refer to square spots of streets (colored with white color), while cell values of the matrix below the specified threshold value refer to square spots of the area outside the streets (i.e., buildings, obstacles, etc.) representing non-accessible points (colored with black color). The application of this procedure results to a 2D matrix full of 0 and 255 and a corresponding black-white image that represents the initial image with streets colored with white color and buildings colored with black color, see Fig. 2c.
4. Considering the two-dimensional matrix full of 0 and 255 the actual graph-construction procedure begins by transforming each particular cell whose value is 255 (i.e., a cell that represents a square spot of the street) into a vertex of the graph. Alongside the creation of the graph vertices, the same procedure constructs the edges of the graph considering the neighbors of the cells, taking into account the 7-neighborhood, that also have value equal to 255. The result is a detailed graph-based representation of the initial image, denoted as  $G_{map}$ , whose vertices represent the actual square spots of the streets, while its edges represent the transitions (i.e., steps) among them. In Fig. 3a and b it is presented an illustrative example of transforming an initial matrix

(i.e., a black-and-white image) into its corresponding graph joining the neighboring cells according to the 7-neighborhood by adding an edge among their corresponding vertices.

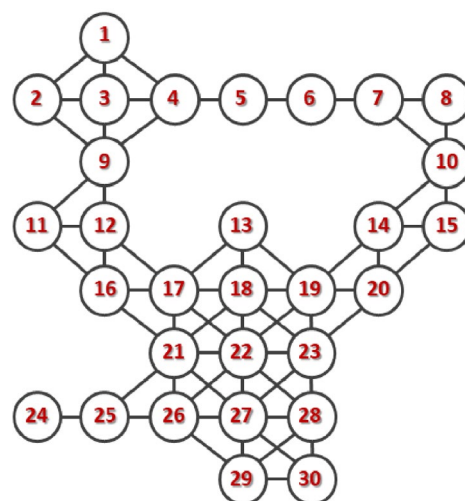
### 2.2.2 Assign points of interests

To make our model more realistic, we consider factors related to the high traffic and the mobility of any particular city. Points of Interest or “attraction points” in a city are frequented streets or high-level traffic areas which increase the congestion and hence the hyper-transmission of the airborne pathogens. In our proposed simulation framework, the user assigns the Points of Interest (or, for short, PoI) at the start of the experiment, by marking with red color these regions in the black-and-white image representing the high traffic areas of the city, see Fig. 2d. To this point, it is of major importance to notice that only the non-accessible points of the image (i.e., buildings and obstacles) need to be marked to assign the importance level that denotes the Points of Interest. At the end of this procedure, to simulate the traffic of the initial city’s roads, our proposed model constructs a new matrix, the so-called *Attraction-Matrix*, whose cells correspond to square spots of the streets with a value from a specific range of numbers (from 0 to 10), where the higher the value of the cell, the more frequent the square spot of the street is.

In our model, we distinguish the street spots according to their congestion (i.e., their distance from their nearest PoI) as follows:



(a) Initial Matrix.



(b) Resulting Graph  $G_{map}$ .

**Fig. 3** Example of converting a matrix to its corresponding graph taking into account the 7-neighborhood of its cells

- a **hot spot**, a square spot of the street which is very close to its nearest PoI, where its corresponding cell in the Attraction-Matrix ranges between 10 and 7, i.e., (7, 10], according to its distance from the PoI.
- a **warm spot** a square spot of the street which is not very close its nearest PoI, where its corresponding cell in the Attraction-Matrix ranges between 7 and 4, i.e., [7, 4], according to its distance from the PoI.
- a **cold spot**, a square spot of the street which is away from its nearest PoI, where its corresponding cell in the Attraction-Matrix ranges between 4 and 0, i.e., (4, 0], according to its distance from the PoI.

Hence, once the PoI have been marked with red color in the black-and-white image, we compute the significance of each particular cell of the Attraction-Matrix, which corresponds to a square spot of the street considering its distance from its nearest PoI, and accordingly the cells will be defined as hot, warm, or cold spots based on their distance from their nearest PoI. In Fig. 4a there are represented the hot, warm, and cold spots, marked with orange, yellow, and purple color, respectively, according to their distance from the closest PoI, as they are located in specific regions of the modeled area (see, Fig. 2d). To this end, it is worth noting that in our model the Attraction-Matrix is a component of major importance in the construction of the route basis and the determination of which path each individual follows, moving from a source to a destination point in the city.

### 2.2.3 Constructing the route basis

Considering the undirected graph  $G_{map}$ , each vertex represents a square spot of the street and corresponds to a cell of the Attraction-Matrix. At this point, to construct the route

basis, we need to reconstruct the weights of the edges of the underlying undirected graph, that so far have weights equal to 1, considering the PoI that have been set, recalling that its vertex-set corresponds to street spots and its edge-set corresponds to their in-between neighbors (7-neighborhood). The new weight for an edge  $e_{i,j} \in E(G_{map})$  connecting the vertices  $v_i, v_j \in V(G_{map})$  is calculated as:

$$w(e_{i,j}) = 10 - L_i + 10 - L_j + 1, \quad (1)$$

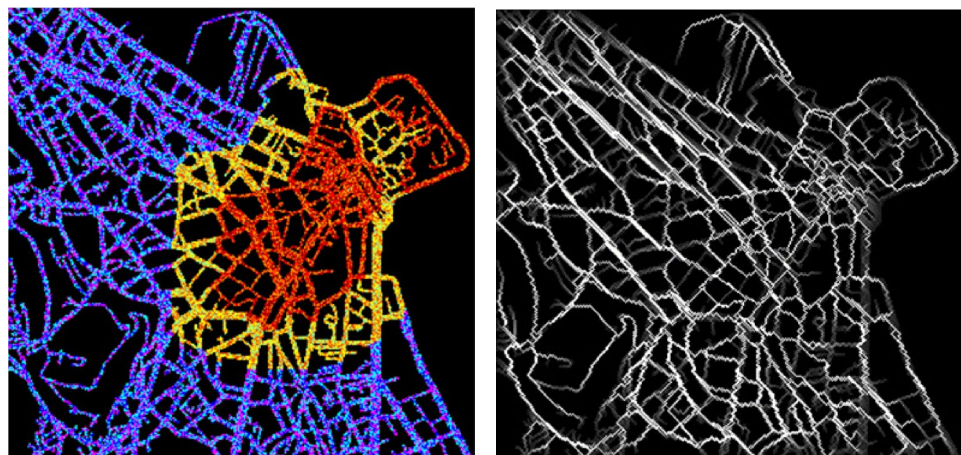
where  $L_i$  and  $L_j$  are the Attraction-Matrix cell's values (i.e.,  $L_i, L_j \in [0 - 10]$ ), based on the vertices  $v_i, v_j$  connected by the corresponding edge  $e_{i,j}$ .

To this point, it is important to note that in the end of the procedure all the weights of the graph will be recalculated, and according to our formula their corresponding values will be set in the range [1, 21]. Hence, the proposed model reconstructs the edges of the undirected graph  $G_{map}$  considering the PoI of the image based in Equation 1 to construct the basis for the possible routes (see, Fig. 4b).

## 2.3 Mobility model

Our proposed mobility model is developed to simulate the movements in terms of mobility patterns of the individuals, the frequency of their walks and the paths they select to follow to reach their destinations, as they consist major factors that affect the dynamic density of the city's network considering the congestion of the individuals in particular regions of the city area, and to a further extent to the dynamics of the spread of on airborne pathogen. Next, we describe the scheduling of the individual's mobility patterns (i.e., route basis) as also the algorithms used to compute the paths followed by the individuals.

**Fig. 4** Example of Hot, Warm, and Cold Spot assignment (a), and visualization of frequently walked streets by the mobility of individuals



(a) Assignment of Hot, Warm, and Cold Spots.

(b) Visualization of frequently walked streets by the mobility of individuals.

### 2.3.1 Scheduling the mobility of individuals

Considering that the mobility of the population inside a city area is not totally random, and taking into account that rush hours may differ across different cities, the proposed model is flexible enough to support variations exhibited in any hour peaks, according to simulation demands, w.r.t. the city under consideration. More precisely, every single individual has a probability to start a route at any time during the day from a source point of the city to a random destination point. The probability for each individual to start moving into the city increases or decreases according to the percentage of the population estimated regarding specific time-periods in a day (i.e., rush hour or not). In Fig. 5, we illustrate the congestion of the streets based upon the hourly mobility of citizens representing the congestion in the streets of a city, where, utilizing data collected by the national organization for transportation, in the  $x$ -axis there are depicted the time-periods of a day in hourly basis; while in the  $y$ -axis, it is presented the percentage of the population moving inside a city area across these time periods in a day.

Next, we discuss the procedure that describes the assignment of the source and the destination points defining the paths to be followed by each individual (i.e., the routes that model the mobility patterns of the individuals inside a city area), how points of interests affect those paths, as also possible alternative route assignments as long as a path has already been set.

- **The effect of Hot-Spots in the routes followed by the individuals.**

Given a source and a destination point as vertices of the  $G_{map}$ , the proposed mobility model allows each individual to select the less weighted (i.e., shortest) path among all possible paths that connect these source–destination points. Given a source and a destination point, the shortest, and hence the less weighted, paths in our graph

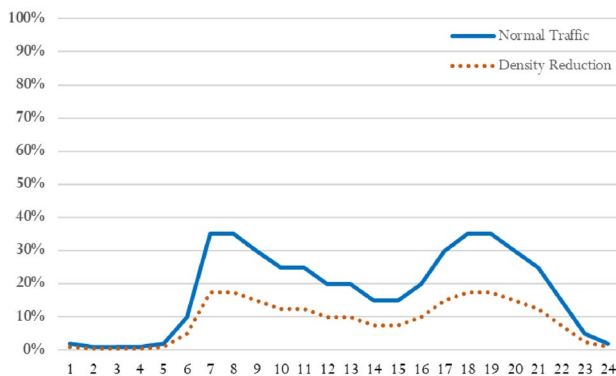


**Fig. 5** Hourly congestion in population mobility inside the boundaries of a city

result, thus, to the most frequently walked paths of the city (see, Fig. 4b). Additionally, it is of major importance to note that this approach corresponds these paths to the paths that utilize the edges among the spots with greater values, or, equivalently to the paths that contain the edges that are included in most of the paths. To achieve this, we use Dijkstra’s shortest path algorithm (Dijkstra 1959) for every individual who decides to move from a source to a destination point of the graph, ensuring hence that the selected path includes the less weighted edges.

- **Stochastic assignment of source–destination points.**

As long as the points of interests have been set and the weighted edges of the graph have been reconstructed, our system assigns to each individual a static source point that remains immutable, representing, e.g., the residence of an individual. The source point of an individual is a point in the map that the individual starts and finishes the most of the routes representing the location of the home. Then, iteratively over specific periods of time, every individual has a probability to make an action (i.e., to define a path between its source and a random destination point and start the corresponding route through the city) depending on the corresponding state (i.e., “stand”, or “move”). At the beginning of a time-period, all the individuals are located at their residences (i.e., home locations), so each individual computes based on a probability on whether to stay at home or to start a route in the next time-period. Additionally, in terms of simulation, a “period” refers to the simulation of a day (*simulation day*), while the “time-period” refers to the next hour (*simulation hour*). Then, each individual whose route is scheduled to start, a random time-slot ranging from 1 to 60 minutes from the current time (in our case, 1 – 500 simulation steps correspond to one hour of the day) is assigned, to start its route. Moreover, it is worth noting that when the individual is about to move, w.r.t the time defined by the assigned time-slot, a random destination point of the city’s map is assigned to construct the route of an individual that is about to move. Once the destination point has been set, we deploy Dijkstra’s shortest path algorithm (Dijkstra 1959) to calculate the shortest path in the graph and navigate the corresponding individual between source and destination points via the shortest and less weighted path.

- **Optional selection of performing sequential routes.**

The proposed mobility model decides whether a individual starts a route or not, within a proximal time-period w.r.t the probability defined for the corresponding time intervals depicted in Fig. 5. Focusing on possible actions that may occur during the route of an individual, when it is time for an individual to start a route, the proposed mobility model calculates the shortest path and the corresponding individual is placed onto the vertex of the graph

that represents the source point (i.e., residence of this individual) in the city. To this point, in every simulation step the individual moves from the current vertex of  $G_{map}$  to one of its neighboring vertices, and more specifically, to the next vertex that Dijkstra’s algorithm undermines for the corresponding path. However, during the navigation on the streets, as in reality, there is a probability of “meeting another known individual” who also follows the route probably to its own destination point into the graph (e.g., routes from pairs of different source–destination pairs that are crossed, or, more formally, paths with joint vertices or edges). In that case, both individuals will stay at the same vertex for 0–5 time-slots and then they will continue their navigation to their corresponding destination points. In our model, to construct such a contact-network, we construct a random graph (i.e., *Friendship Graph*) of order equal to the population of the modeled city, depicting the friendships among the individuals. This procedure reflects a real-life scenario where two people that know each other randomly meet in a city’s street and stand-by for at least a handshake, or a short talk. As long as the individual reaches the destination point of the city, remains stable to the corresponding vertex of the graph for a specific period of time (likely to the real life, e.g., to perform a task) and then decides one of the following actions, i.e., whether to move to a new destination point of the city (e.g., to perform another task), or to return home (i.e., the new destination point is reset to the initial start point).

## 2.4 Propagation model

Next, we present the third model of our framework, i.e., the propagation model, discussing the underlying epidemic properties that describe the potential states an individual may be during the spread epidemic, possible actions of each individual that affect the transmission of an airborne pathogen, and the evolution of the viral load inside the organism of an infected host regarding the exhibited symptoms, affecting the infection ability of the infected host.

### 2.4.1 Underlying epidemic model

The proposed approach for the modeling of the spread of an airborne pathogen has its structure based on the characteristic behavior exhibited by the pathogen considering its transmission. The proposed integrated simulation framework incorporates the S–E–I–R compartmental epidemic model, including the states (Susceptible–Exposed–Infectious–Recovered), where each individual can be in one of them as follows:

1. **Susceptible:** individuals have never hosted the pathogen, being, hence, susceptible to it,
2. **Exposed:** individuals that got infected by the pathogen but are not yet contagious,
3. **Infectious:** individuals who are infected by the pathogen and are contagious, and
4. **Recovered:** individuals that have recovered, and being neither Susceptible nor Infectious, they do not transmit the pathogen.

Investigating the states that are critical for the contagion of the virus, in this work we study four possible actions that can be performed by any individual to transmit an airborne pathogen. Namely, the possible actions considered by our model are *breathing*, *coughing*, *sneezing* and *talking* and each one has a specific probability of being performed at any time. The corresponding percentage of the viral load to be propagated through the infected emitted droplets is analogous to the evolution of the viral load inside the infected host. The probability of each action differs according to the epidemic state of each individual, as also to the corresponding viral load and the characteristics of the pathogen under consideration, in our case the SARS-CoV-2 virus. For example, an infectious individual exhibits an increased probability of coughing compared to an individual whose state is susceptible. In addition, the percentage of the viral load contained in the droplets emitted through an action performed by an individual is also relative to the epidemic state and the corresponding viral load. Moreover, the probability of performing an action and the amount of the viral load transmitted by the emitted droplets varies among individuals of the same epidemic state according to the evolution rate of the viral load inside different hosts.

In Tables 1 and 2, we provide an estimation of the probability of an individual to perform an action that transmits a portion of infected droplets that carry the airborne pathogen and additionally, we present an estimation on how this probability evolves across the evolution of the viral load inside an infected individual, and the corresponding percentage of infected droplets, respectively. In our approach, regarding the spread of emitted droplets, we utilize the data and approaches presented in (Dhand and Li 2020; Seminara et al. 2020; Anand and Mayya 2020; Katre et al. 2021).

**Table 1** Probabilities of actions performed by healthy (susceptible) individuals and corresponding volume of emitted droplets

Actions performed by an individual:	Breath	Cough	Sneeze	Talk
Probability of performing an action	0.8	0.1	0.05	0.05
Volume of Emitted Droplets (VoED)	0.2 m <sup>3</sup>	2 m <sup>3</sup>	3 m <sup>3</sup>	0.5 m <sup>3</sup>

**Table 2** Probabilities of actions and corresponding percentage of emitted droplets per individual across the evolution of the viral load ( $vI$ )

Viral load ( $vI$ )	Breathing	Coughing	Sneezing	Talking	Perc(ID)
$vI = 0$	0.8	0.1	0.05	0.05	0.1
$0 < vI \leq 10$	0.8	0.1	0.05	0.05	0.15
$10 < vI \leq 20$	0.8	0.1	0.05	0.05	0.2
$20 < vI \leq 30$	0.8	0.1	0.05	0.05	0.2
$30 < vI \leq 40$	0.8	0.1	0.05	0.05	0.2
$40 < vI \leq 50$	0.75	0.15	0.05	0.05	0.3
$50 < vI \leq 60$	0.70	0.20	0.05	0.05	0.4
$60 < vI \leq 70$	0.65	0.25	0.05	0.05	0.5
$70 < vI \leq 80$	0.60	0.30	0.05	0.05	0.6
$80 < vI \leq 90$	0.55	0.35	0.05	0.05	0.7
$90 < vI \leq 100$	0.50	0.40	0.05	0.05	0.8

Concerning the distribution of probability values on performing an action (breath, cough, sneeze, talk) as they are presented in Tables 1 and 2, since to the best of our knowledge there does not exist yet any relative work in the literature regarding the probability values of performing such actions with respect to the SARS-CoV-2 symptoms, they are initially defined intuitively, as they are presented in Table 1, while later, as presented in Table 2, the probability distribution alongside the corresponding percentage of infected respiratory droplets are modified according to the increase of the viral load.

In particular, in Table 1 we present the probability of an individual to perform one of the set of basic actions that mostly favor the transmission of an airborne pathogen through the emitted droplets, namely breathing, coughing, sneezing or talking, alongside the corresponding volume of emitted droplets per action, denoted by  $VoED$  that are spread at a specific distance (Katre et al. 2021; Bahl et al. 2020; Seminara et al. 2020). In Table 2 we present the evolution of the viral load ( $vI$ ) inside an infected individual represented with values in the range  $[0, 100]$  (see, column 1), the corresponding probabilities of performing an action that emits droplets (see, columns 2-4), and finally, concerning the evolution of the viral load inside the host

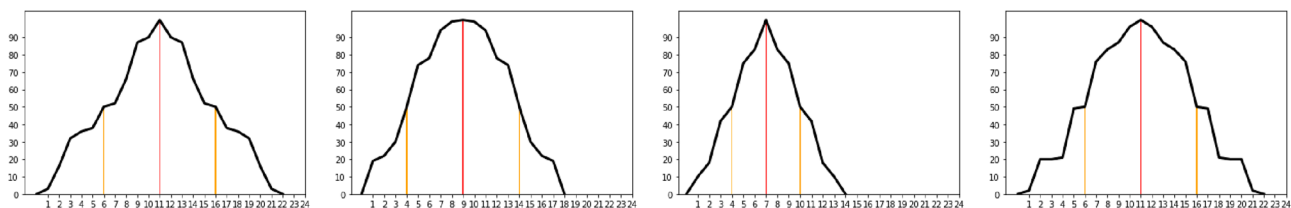
individual, the corresponding percentage of infected droplets  $Perc(ID)$  emitted that are independent of the performed action (see, column 6). Thus, according to this approach, in our propagation model at each time-slot of our simulation each individual has a probability of performing an action, and according to its epidemic state and its viral load evolution that we will discuss later, and stochastically to transmit the airborne pathogen.

#### 2.4.2 Stochastic evolution of the viral load inside hosts

Next, we discuss how the immune system in each individual behaves while hosting the airborne pathogen from the start of infection and how the corresponding viral load evolution varies inside different hosts and hence different immune systems, as it is of major importance to contain the aspect that the same pathogen may cause different results to different individuals. For example, the viral load evolution in an individual with chronic deceases is more aggressive than a healthy person who got infected.

To include this case in our model, we assign to each individual a “behavioral profile”, representing the viral load evolution by the time of infection. The corresponding viral load evolution curve that depicts this behavioral profile represents the information regarding the increasing ratio of the virus into the corresponding host, the first day of the symptoms and the viral load distribution during the days of being in the infectious state. The constructed curves stochastically vary and they have been developed focusing to simulate different behaviors of the viral load evolution through different individuals. At the end of this procedure, we achieve the different confrontation of the virus on each individual maintaining the base features of the corresponding virus.

As long as a susceptible individual gets infected, the stochastically developed behavioral profile describes the viral load evolution during the days, determining the incubation period, the first day of symptoms, the day that the viral load reaches its peak and the cure day. In Fig. 6 we illustrate four different stochastically developed behavioral profiles, e.g., for four different individuals, describing the evolution of the viral load when hosting the pathogen during the days after their infection. In particular, in Fig. 6 the  $x$ -axis refers

**Fig. 6** Different curves that describe the evolution of the viral load inside different infected individuals, where the  $x$ -axis refers to the days after the infection and the  $y$ -axis refers to the evolution of the viral load ( $vI$ ) inside the infected individuals

to the days after the day of infection and the  $y$ -axis refers to the percentage amount of the viral load ( $v_l$ ), while the three vertical lines indicate the critical points during the evolution of the viral load regarding the first day of symptoms, the day that the viral load reaches its peak, and the cure day.

Taking into account the results presented by (Lippi et al. 2020), we stochastically simulate the curve of viral load evolution estimating that a host is about to reach a 50% of the viral load exhibiting the first symptoms 3–6 days after the infection. From the day of symptoms onset, there is a margin of 3–6 days for the viral load to increase until its peak. In our model, we consider that the decrease ratio of the viral load curve equals the corresponding increase ratio. As long as the percentage of the viral load of the corresponding infected individual increases, the probability for coughing and the percentage of the infected respiratory droplets increases analogously. As a result, the individual becomes even more contagious and the probability to transmit the pathogen increases too.

Finally, an infected individual is considered to be infectious stochastically by a maximum of 2 days before the symptoms onset, i.e., depending on its stochastically developed viral load evolution curve, approximately at 30 – 40% of its viral load evolution. More precisely, in our approach regarding the simulation of the transition from one compartment to another, an infected (exposed) individual is considered infectious from the next day after the day of infection, where the probability of infecting other individuals is very low due to the low value of viral load, which affects the transmission through the stochastic performance of each action. In our approach, the infected individual is considered to remain infectious in a symmetrical range after the pick of its viral load evolution, i.e., when the viral load has been reduced to 30 – 40% after its peak.

### 2.4.3 Infection of proximal population

Modeling the aspect of infection of proximal population, we focus into the physical substance of the procedure that describes the transmission of an airborne pathogen from an infectious individual to the nearby susceptible ones. Airborne pathogens spread through the air via respiratory droplets produced after an action performed by an infected individual (i.e., talk, breathe, cough, sneeze). The quantity of the produced droplets is proportional to the action performed, while the radius of each droplet can vary, depending on the intensity of the corresponding action, i.e., the produced droplets after a sneeze are up to 40000, while coughing may produce up to 3000 (Katre et al. 2021; Anand and Mayya 2020; Dhand and Li 2020; Seminara et al. 2020).

Investigating the insight of this procedure, the proposed model considers the increased spread of the droplets over distance as the droplets transition in the air can be described

as a “triangular cloud” (Seminara et al. 2020) whose one corner located in front of the infected individual, where the droplets released. To make our model more realistic, we consider the orientation of each individual into the  $G_{map}$  graph developing over each individual a triangular cloud inside the boundaries of which the pathogen can be transmitted through the droplets emitted through an action performed by the infected individual.

To simulate the transmission of the airborne pathogen and the infection of proximal population we need to consider the distance among them, the viral load and the type of the action performed (i.e., breath, talk, cough, sneeze). Hence, to meet this requirement, we developed a formula to calculate the probability of infection incorporating these three factors. The probability of an individual  $X$  to get infected  $P(X \rightarrow Infected)$  decreases as the distance from nearby infected individual  $Y$  increases, while, respectively, increases as the amount of viral load and the quantity of infected respiratory droplets emitted by a nearby infectious individual are increased  $Y$ . In our model, we compute the probability of a susceptible individual  $X$  to get infected by a nearby infectious individual  $Y$  considering its viral load amount and the action performed as:

$$P(X \rightarrow Infected) = \frac{Perc(ID) \times VoED}{1 + Eucl(X, Y)^2}, \quad (2)$$

where  $Perc(ID)$  corresponds to the percentage of infected respiratory droplets a nearby infected individual emits by an action,  $VoED$  corresponds to the volume  $V$  of the emitted droplets a nearby infected individual emits by an action, and the  $Eucl(X, Y)^2$  corresponds to the square of their in-between Euclidean Distance.

To this point, we should note that if  $Y$  is not infectious then the probability  $P(X \rightarrow Infected)$  is eliminated since  $Perc(ID) = 0$ , as also if the amount of viral load is very low or  $X$  is away from  $Y$ , or even both, accordingly it holds that  $P(X \rightarrow Infected) \approx 0$ . In Fig. 7, we combine the information from Table 1, Table 2, and utilizing Equation 2 we represent the probability of infection of a susceptible individual that has a safety distance of  $2m$  (Bahl et al. 2020) from a nearby infectious individual.

Finally, in Fig. 8, we illustrate an example of the utilization of the proposed model. Particularly, in Fig. 8a, there are depicted the positions of the individuals inside the city area, where the green marks correspond to the susceptible individuals and the red marks correspond to the infectious individuals. In Fig. 8b, there are depicted the triangular clouds that contain the respiratory droplets emitted through the actions performed by the infectious individuals towards their direction according to their moves, while in Fig. 8c, we represent with pink marks the points of the area where the infections were recorded according to our simulations

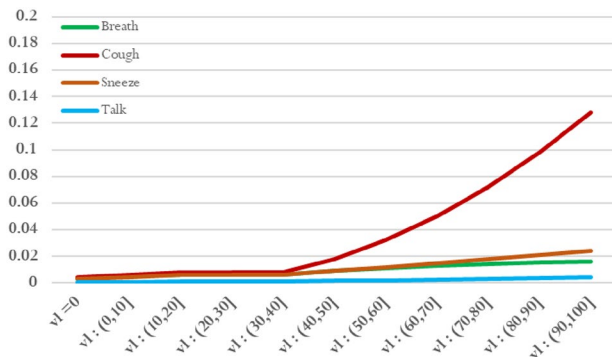


**Fig. 7** Probability of infection by a nearby host at distance  $2m$  according to Tables 1, 2, and Eq. 2

experiments. To this point, it is of major importance to note that the accumulation of the points where infections were recorded exhibits an identical density exactly over the most frequently walked street points (see, Fig. 4b), which is a fact expected from our reality-based intuition, validating thus the accuracy of the integration of the proposed spatial, mobility, and propagation models into a unified simulation framework.

### 3 Integrating the simulation framework

In this section, we present the basic components over the development of our proposed integrated simulation framework for pandemic prevention and mitigation regarding its design principles, the modeling of the spread of an airborne pathogen, in our case the SARS-CoV-2, in an uncontrolled environments (i.e., in an environment where no countermeasures are taken to prevent the pandemic, e.g., no face masks, no safety distances, etc.), and the approaches

(i.e., countermeasures) that will be utilized to mitigate the epidemic.

#### 3.1 Design principles

In the basis of our experiments to simulate the spread of the airborne pathogen we consider the main scenario, where people are not aware of the consequences of the spread of the airborne pathogen (uncontrolled environment) and the scheduled routes of individuals are irrelevant to their state. For example, an infectious individual will move across the city performing the scheduled routes until the end of the experiment, even if he has fever or is symptomatic hosting and transmitting the pathogen. To this end, it is important to note that spatial model for a specific city and the propagation model for a specific airborne pathogen remain both unchanged in every different case that we approach in our experiments, while the mobility model is differentiated adapted to any countermeasure we investigate in each series of experiments to study its effect on pandemic prevention. Through the range of countermeasures that we investigate regarding its potentials into mitigating the epidemic, there is the reduction of the population density that moves inside the city area, the self-isolation, the contact tracing, the implementation of efficient algorithmic tracing techniques, as also combinations of them.

#### 3.2 Modeling the spread in an uncontrolled environment

To model the spread of a virus in an uncontrolled environment, we create the corresponding weighted undirected graph  $G_{map}$  from the initial Google Maps image including the PoI that affect the citizens' routes (see, Sect. ) and model the individuals to navigate through it following random

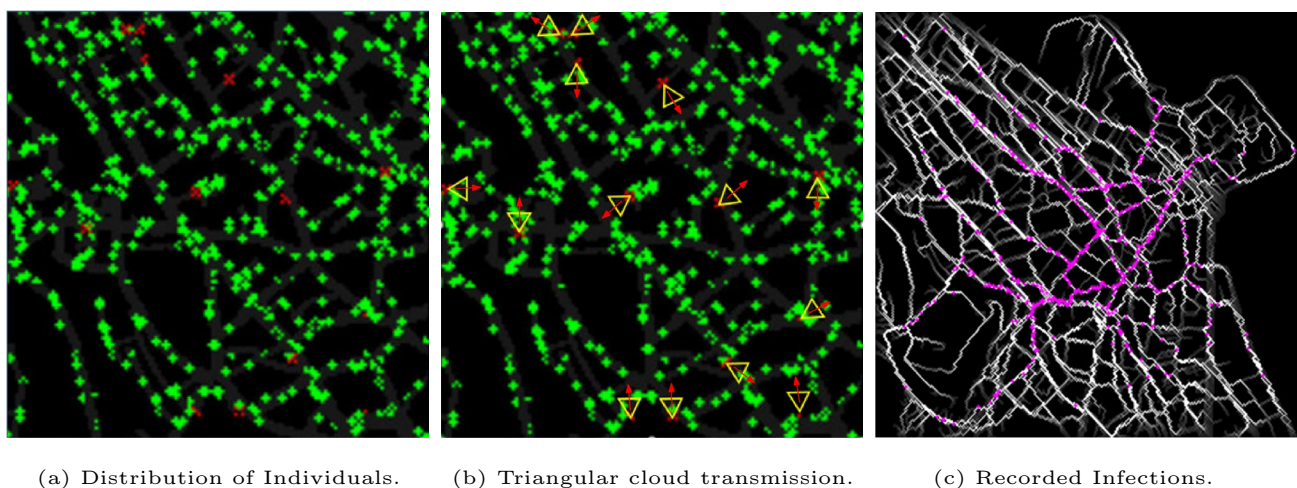


**Fig. 8** Airborne virus transmission from nearby infectious individuals in a specific area of the city, and points of registered potential infections

walks. The frequency of each individual's routes is developed according to the corresponding mobility data (see, Fig. 5), ranging from 3 to 4 routes per day while this number remains unchanged throughout all the series of experiments regardless the state of the corresponding individual. During a simulation day, as long as the individuals move through the city they may take one of the respiratory actions (i.e., breathing, coughing, sneezing, talking), spreading hence the airborne pathogen to their nearby susceptible individuals, if they are infectious and analogously the evolution and the amount of their viral load. The pathogen propagation in each infected individual described from the viral load evolution which defines how contagious the corresponding individual is.

### 3.3 The effect of density reduction

To reduce the spread of the airborne pathogen or even prevent a possible pandemic we implement in our simulation model, and more specifically in the corresponding mobility model, the deployment of the countermeasure of "density reduction". The construction of the spatial model and the propagation model remain both the same since we examine the spread of the same airborne pathogen in the same area and the same population. The aim of this implementation is the reduction of the spread of the pathogen decreasing the density of the population residing and moving through the specified area. To achieve this, we allow at most the 50% of the individuals (see, Fig. 5 red dotted line) that consisted the moving individuals in any hour of the day as described in the initial mobility data (see, Fig. 5 blue line) to move through the city during a day. For example, at 12:00 in the corresponding mobility representation of the first experiment (i.e., uncontrolled environment) approximately 20% of the total population move inside the city performing their scheduled routes. Applying the countermeasure of "density reduction" at 50%, if an individual has scheduled a route at 12:00 and a 10% of the population are moving inside the city area, the corresponding individual will cancel the route (i.e., delaying the route until the next available time-slot) ensuring that the percentage of the individuals that are moving inside the city area at that specific time does not exceed the 10% of the total population.

### 3.4 Flatten the curve through spread awareness

A commonly used countermeasure to reduce the spread of an airborne pathogen is to set in quarantine the infected individuals for a period of time to be cured and limit the spread over the susceptible population. In our approach, we assume that every individual will be set to quarantine after 2 days from the appearance of the first symptoms (i.e., symptoms onset is considered when the viral load curve of

the corresponding individual reaches 50%). The quarantine lasts 10 days (Organization 2021; Center for Disease Control and Prevention 2020), and during this time the corresponding individual is unable to move outside the residence, or to contact with other individuals, and hence unable to spread the disease. When the quarantine expires for an individual, the corresponding epidemic state changes from infectious to immune and is able to move again in the city area.

Based on our previous approach and deploying the main principles of infection tracking, we consider the utilization of contact tracing applications (Akinbi et al. 2021) regarding the close contacts (Cortellessa et al. 2021), utilized through smart mobile devices that can track their locations using GPS and Bluetooth 4.0 or higher, in order to register the spatial positions of the individuals along their routes (see, Fig. 8c) and hence registering their contacts to assist the tracking of infections reducing to a further extent a potential pandemic. In our case, we consider that every individual uses a mobile application, like the one proposed by (Chondros et al. 2021), which is responsible for tracking the close contacts during the daily routes, registering them into a centralized data-base. Throughout the implementation of such an approach, and considering that contact tracing applications can store the duration of each contact with a particular individual, a contact of an individual is defined as any other individual appearing in a range of 10 meters (i.e., in our case, 10 street spots or, equivalently, located at any vertex of distance  $d : d \in [0, 10]$  in the corresponding  $G_{map}$  graph) from the individual if the accumulated duration exceeds a time period of 12 minutes, w.r.t. the simulation time. In this context, we assume that each individual will be set to quarantine two days after symptoms onset alongside the contacts made during the last two days (i.e., simulation days).

As long as an individual that has been detected as infected is set to quarantine and all the paths scheduled for this individual are canceled, being unable to move through the city for a period of 10 days and hence not being able to transmit the pathogen to other susceptible individuals. When quarantine expires, the corresponding individual is able to schedule new routes and move through the city according to the mobility model with one of the two possible states, i.e., if the corresponding state of this individual was susceptible the time had been set to quarantine (probably as a contact of an infected individual) then the corresponding state remains the same at the expiration of the quarantine, otherwise (i.e., if this individual was detected as infected) the state of this individual will be set to immune.

### 3.5 Augmenting the contact tracing procedure

One of the main concerns over the procedure of contact tracing is primarily to locate as soon as possible the close contacts recently made by an individual that has been detected

as infected (i.e., the contacts made the past two days before symptoms onset, or the testing date). To this direction, we have designed and propose the deployment of an algorithm, the *2D-Co-Contact Algorithm*, that is intended to extend this procedure to a wider range of individuals including the contacts this individual made the last two days as in the traditional contact tracing procedure alongside the current contacts of the contacts an infected individual made two days ago (namely, contacts-of-contacts, or, for short, *Co-Contacts*). The main intuition behind the design of this algorithm is that if an infected individual, let  $P_i$ , has already infected some of the contacts made two days ago, let  $C_{i,k}, \dots, C_{i,l}$  then these contacts and especially the less recent, i.e., the ones made two days ago, let  $C_{i,l-1}$ , currently should be infectious, and hence the contacts they made the current date (i.e., second-degree contacts, or *Co-Contacts*), let  $C_{l-1,q}, \dots, C_{l-1,r}$  should also be set to quarantine as potentially infected as also the immediate contacts  $P_i$  made during the last two days.

---

**Algorithm 1** The *2D-Co-Contact Algorithm*.
 

---

**Input:** List of Contacts of the Last 2 Days

**Output:** List of individuals to be set to Quarantine

---

```

1: Initiate the List of Contacts to be notified regarding the individual under
   consideration.
2: while The list of contacts is not null do
3:   Select current contact;
4:   Add this person to the List of Co-Contacts to be set to Quarantine;
5:   if The date of contact between the infected individual and this
       individual (current contact) is exactly two days before then
6:     Retrieve the contact list of this individual including the contacts
       made the last two days including the current day;
7:     while the list of contacts of this contact is not null do
8:       Select a contact;
9:       if The date of contact between this contact of the infected
           individual and this individual is the current date. then
10:        Add this person (i.e., contact of the contact - Co-Contact)
           to the List of Co-Contacts to be set to Quarantine;
11:       end if
12:       Proceed to the next contact;
13:     end while
14:   Proceed to the next contact;
15: end if
16: end while

```

---

Throughout the procedure described, for each individual we propose and deploy the *2D-Co-Contact Algorithm*, as presented in Algorithm 1, utilizing its contact list that includes its contacts from the last two days. Next, the contacts made exactly two days before the symptoms onset, are more like to have already an adequate viral load in the current date being infectious enough to transmit the disease to the contacts they made in the current date. Hence, for each individual we select from the corresponding contact list the contacts made two days before the date that the symptoms appeared, and for each one of these contacts we scan its corresponding contact list, (i.e., the contact list of this contact), and select the contacts they made the current date (i.e., *Co-Contacts*). We store all these individuals in a list alongside

the contacts the infected individual had the last two days, and return it as output of the algorithm in order for our system to notify them through the mobile application (Chondros et al. 2021) as to be isolated. To this point, it is obvious that the more the contacts an infected individual had, the more *Co-Contacts* should be notified and to a further extent to be set in quarantine. However, despite the wide range of individuals this approach covers by extending one step further the traditional contact tracing procedure, it seems to provide a quite promising solution to the mitigation of the disease spread, exhibiting better dynamics and scaling with respect to the potentials of effectiveness compared to the traditional contact tracing procedure.

In Fig. 9, we present a clear illustration on the transmission of an airborne pathogen from the patient zero, denoted as  $P_0$ , to its contacts, denoted as  $C_m, \dots, C_n$ . Based on the states of the SEIR epidemic model, we mark with green color the susceptible individuals, with orange color the infected (exposed) but not yet infectious individuals, and with red color the infectious individuals. Throughout the example of Fig. 9, we do not utilize the repaired state since it does not concern the case study of contact tracing. As we can observe from Fig. 9, in day 0 the currently infected but not infectious  $P_0$  has a suspicious contact with individuals  $C_1$  and  $C_2$ , where the pathogen has an almost null probability to be transmitted since the viral load in  $P_0$  is very low. In contrast, in day 1  $P_0$  transmits the pathogen to its contacts  $C_3, C_4$  and  $C_5$ . In day 2,  $P_0$  transmits the pathogen to its contacts  $C_6$  and  $C_7$ , while the suspicious contacts of previously infected but not yet infectious  $C_3, C_4$  and  $C_5$ , also have a nearly zero probability to get infected by them. Finally in day 3,  $P_0$  transmits the pathogen to its contacts  $C_8, C_9$  and  $C_{10}$ , where we assume that at a later time in that day  $P_0$  is notified as being infected proceeding with the deployment of the contact tracing procedure. To this point, it is where the *2D-Co-contact Algorithm* is differentiated from the traditional contact tracing procedure that retains solely the contact of the last two days and the current day's contacts, providing a much more effective approach to proactively ensure the mitigation of the epidemic and to a further extent its elimination.

In Table 3, we provide the corresponding contact lists created by the detection of  $P_0$  as infected by the pathogen. In the first row, we provide the result of the traditional contact tracing procedure, while in the second row the ones provided by the deployment of the *2D-Co-Contact Algorithm*, where for an individual  $k$ , we denote as  $\{C_1, C_2, \dots, C_n\}_k$  its contact list for a specific day. As we can observe through Table 3, the deployment of the traditional contact tracing procedure results to a contact list containing the individuals  $C_3, C_4, \dots, C_{10}$ , that consist the contacts of the infected individual  $P_0$  during the last two days and the day that has been detected as infected. On the other hand, as we can observe from Fig. 9 in the third day, where the infected contacts of  $P_0, C_3, C_4$  and  $C_5$  have

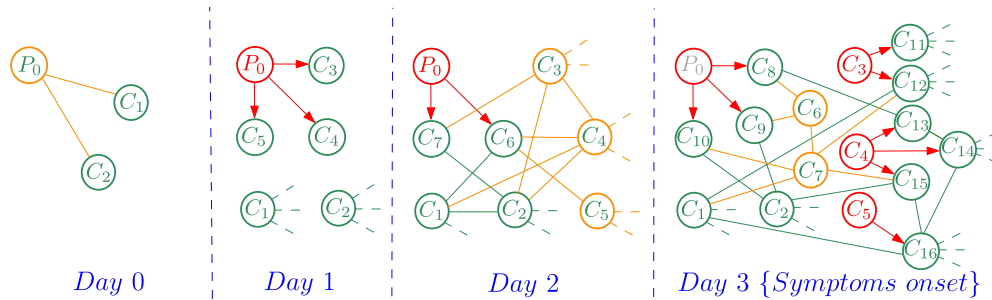


**Fig. 9** Transmission of the disease and contact visualization

**Table 3** Creating the contact list after the deployment of the traditional contact tracing procedure and the contact tracing procedure with the utilization of the 2D-Co-Contact Algorithm

Contact tracing	Current day	Day-1	Day-2
Traditional approach	$\{C_8, C_9, C_{10}\}_{P_0}$	$\{C_6, C_7\}_{P_0}$	$\{C_3, C_4, C_5\}_{P_0}$
2D-Co-contact	$\{C_8, C_9, C_{10}\}_{P_0} \cup \{C_{11}, C_{12}\}_{C_3} \cup \{C_{13}, C_{14}, C_{15}\}_{C_4} \cup \{C_{16}\}_{C_5}$	$\{C_6, C_7\}_{P_0}$	$\{C_3, C_4, C_5\}_{P_0}$

developed enough viral load to transmit the airborne pathogen the deployment of 2D-Co-Contact Algorithm acts proactively, extending the contact list developed over the traditional contact tracing procedure, by adding the contacts that  $C_3, C_4$  and  $C_5$  had that day, i.e.,  $C_{11}, C_{12}, \dots, C_{16}$  as they have a higher probability of having contracted the pathogen, and hence been already infected. This means that, the earlier two days after (i.e., day 5), the individuals  $C_{11}, C_{12}, \dots, C_{16}$  will already have developed symptoms that will force them to get test and obviously found positive to the pathogen yielding another contact tracing procedure.

The main drawback of the application of the traditional contact tracing procedure is that in this interval, i.e., from day 3 to day 5, these infectious individuals will infect other susceptible individuals spreading the pathogen and making hence the epidemic more difficult to get mitigated. To this end, it is of major importance to note that the deployment of 2D-Co-Contact Algorithm acts proactively to ensure that such cases are eliminated as also that the augmented tracing procedure actually precedes of the traditional in terms of time as individuals, that with high probability may result as infected, have been already set to quarantine ensuring the mitigation of the pandemic.

### 4 Experimental evaluation

In this section, we present the experimental results averaged over a series of simulation experiments, regarding the effectiveness of the investigated countermeasures on the outcome of the epidemic considering several factors that depict the potentials of each countermeasure deployed.

### 4.1 Experimental design

Next, we present a series of simulation experiments conducted utilized the proposed integrated simulation framework, averaging the results concerning the daily infection cases and the accumulation of the infectious population over a period of time. Each experiment has been performed sequentially 10 times (similarly to Monte Carlo simulation experiments) to eliminate the factors of randomness required for the deployment of the mobility and propagation models. In the next subsections, we discuss the behavior of the epidemic spread, and more precisely the effect exhibited by the application of several countermeasures.

In our experimental setup, we have select an area of our city, taken from Google Maps to be utilized in the spatial model as the basis of the routes followed by individuals through the mobility model. Considering the properties and the principals of SARS-CoV-2, we conducted a series of repetitive simulations over a sample of 2000 individuals that is the size of population residing in this area, note that neither safety distance limitations among individuals, nor face-mask application were enforced in the simulation of the spread of the airborne pathogen. In our experiments, we start the simulation with one host of the pathogen, i.e., patient zero  $P_0$ , finishing the simulation experiment whether the susceptible population have been all infected, or when the epidemic has been totally eliminated, i.e., there exists neither infected nor infectious individuals in the total population. Finally, for the experiments to be pairwise comparable, we selected to retain the same duration in each experiment, i.e., 40 days after the first infection. In all the figures that represent the corresponding plots for the results of each series of

experiments the  $x$ -axis represents the time (i.e., the number of days) and  $y$ -axis depicts the number of people that got infected on each day (i.e., new infection cases) or currently infectious population (i.e., accumulated number of individuals in infectious state). We also discuss the reproduction number  $R_0 = (\text{new infection cases})/(\text{current infectious population})$  exhibited in each case, where we should note that being also close enough to the results discussed in (Achaiah et al. 2020), it augments the validity of our proposed model. Finally, throughout our experiments, we consider the case of the spread of the airborne pathogen in an uncontrolled environment as the basis of our experiments being also the main reference point to compare the rest of the experiments regarding the defectiveness of each countermeasure investigated.

In the next series of experiments, we distinguish seven classes of experiments. In the first class, we investigate the spread of an airborne pathogen in an environment where no counter measure is deployed. Having this experiment class as a reference point, next, we deploy a series of experiments regarding the application of several countermeasures, namely, the density reduction of the population in terms of lock-down measures, the self-isolation, the application of the contact tracing procedure through a smart mobile application, the combination of the density reduction and the contact-tracing countermeasures, as also the investigation over the effect of response time, i.e., the time required from the symptoms onset until the individual is alerted triggering the procedure of contact tracing, while finally we also present the results achieved by an algorithmic approach presented in this work regarding an optimization on the contact tracing procedure, utilizing the *2D-Co-Contact* Algorithm.

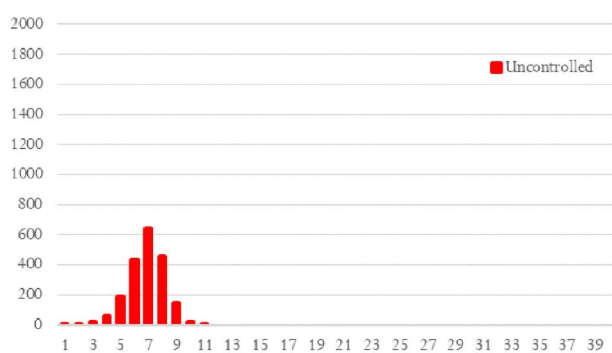
## 4.2 Epidemic spread in an uncontrolled environment

In this series of experiments, we will discuss the achieved experimental results utilizing the proposed integrated

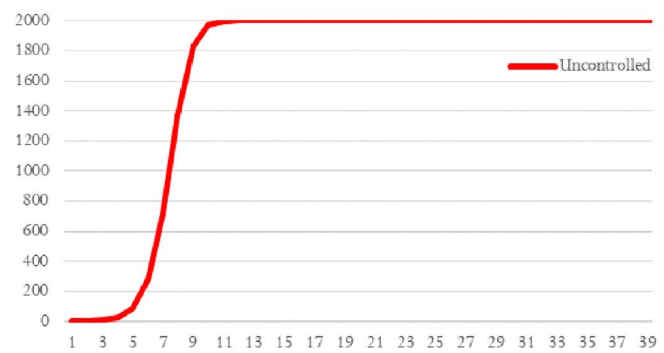
simulation framework, on the transmission of the airborne pathogen in an uncontrolled environment, i.e., where no countermeasures for pandemic control are deployed. The following plots represent the averaged results after a series of simulation experiments for the spread in an uncontrolled environment. We set 1 individual as infected, i.e., *patient zero* denoted as  $P_0$ , and 1999 susceptible individuals moving according to the mobility model into the city. In Fig. 10, we present the exhibited simulation results as long as the spread of the pathogen evolves into an uncontrolled environment. In Fig. 10a, the  $x$ -axis represents the number of days the epidemic lasted, i.e., resulting either to pandemic or elimination, and  $y$ -axis depicts the number of people that got infected each day. In Fig. 10b, the  $x$ -axis also represents the corresponding simulation day and  $y$ -axis, the overall number of people being infectious. As we can see in Fig. 10a and b, our simulation experiments converge to pandemic after the completion of 10 days, with the reproduction number  $R_0$  starting from 2.8 at day 1, reaching a peak of 3.68 at day 3 and reduced to 1.01 at day 10. In Fig. 10a we can observe that the daily infection cases follow a Gaussian distribution, while there is exhibited an increase of the daily infected population until day 7 and a sharp decrease over the days 8, 9 and 10 where the vast majority of the susceptible population have been already infected. Similarly, in Fig. 10b, we can observe a low increase over the 5 first days, an exponential increase of the infectious people until day 9, a logarithmic increase from day 9 to day 10 and a stabilized curve over the next days as long as all the individuals have been infected.

## 4.3 Epidemic control

After the evaluation of our first experiment that consists the reference point to compare the rest of our case-study experiments, we observe that an airborne pathogen with the properties under consideration is not viable as long as all the people of the corresponding city got infected. To prevent



(a) Daily Infection Cases.



(b) Infectious Population Growth.

**Fig. 10** Epidemic spread in an uncontrolled environment where no countermeasures are applied

the pandemic, we need to develop a set of countermeasures and study the effectiveness they exhibit against the spread of the pathogen under consideration regarding the size of susceptible population.

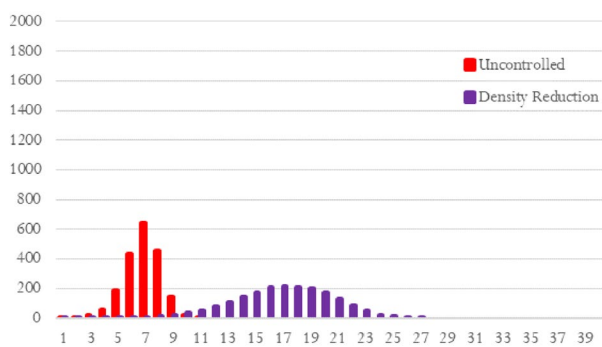
### 4.3.1 Density reduction

Next, we examine the averaged results after a series of simulation experiments deploying the countermeasure of “density reduction” to 50% of the corresponding population in a city. Regarding the achieved results over this series of experiments, Fig. 11a represents the individuals that got infected each day, i.e., daily infection cases, while Fig. 11b represents the accumulated number of infectious individuals from the start of the experiment over each day, exactly as the corresponding plots in the experiments deployed on the spread in an uncontrolled environment. In Fig. 11a and b, we can observe that the experiments converge to pandemic after 27 simulation days, with the reproduction number  $R_0$  starting from 1.8 at day 1, reaching a peak of 1.66 at day 10 and reduced to 1 at day 26. In Fig. 11a, we can observe that, similar to Fig. 10a, the daily infection cases follow a Gaussian distribution with its peak at day 18; while in Fig. 11b, we can observe a sigmoid behavior of the epidemic which increases exponentially from simulation day 13 to day 20 and logarithmically increases from simulation day 20 to 25. At the end of this experiment all the initially susceptible population got infected after 27 simulation days and delay the pandemic, resulting that the implementation of the countermeasure of “density reduction” in our simulation model did not performed adequately well to prevent the pandemic.

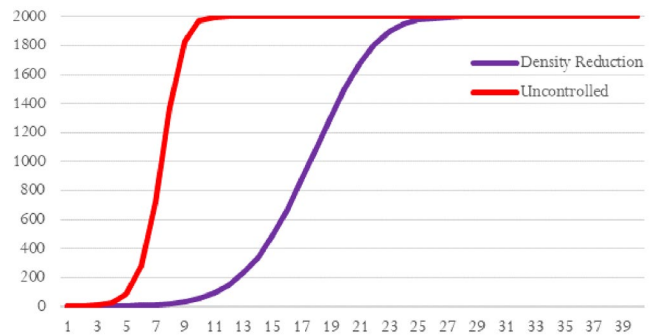
### 4.3.2 Self-isolation

Another popular countermeasure to prevent a possible pandemic is the personal quarantine of the infected individuals

by performing a countermeasure of “self-isolation” to reduce the spread of the airborne pathogen. In our approach, we consider that every individual 2 days after symptoms onset will be set to quarantine for 10 days. At the end of their quarantine, the corresponding individuals have been cured and they return to the population performing their daily walks with their corresponding states as immune. At the end of the simulations of this counter measure, denoted as  $S - Q$ , after observing Figs. 10 and 12, we cannot discriminate a significant difference after its application, since, as we can observe from the results exhibited in Fig. 12a and b, our simulation experiments converge to pandemic after the completion of 10 days, with the reproduction number  $R_0$  starting from 1.66 at day 1, reaching a peak of 3.19 at day 5 and reduced to 1 at day 10. The pandemic prevention failed and the daily infected and the infectious population are similar over the days compared to the results of the spread in an environment where no countermeasure is applied to reduce the spread of the pathogen (see, Fig. 10). This observation results from the fact that during the isolation of a single host of the pathogen (i.e., an individual that has been infected by the airborne pathogen), it does not reduce the spread of the pathogen since its potentially infected contacts are carries of the pathogens that will contribute to its transmission. We can simply consider the case where only the patient zero, let  $P_0$ , is isolated omitting his/her contacts who potentially may be infected by  $P_0$  to continue spread the pathogen. Such an approach would be equivalent to the case where the experiment started from the next day but having a larger group of initially infected population (i.e.,  $> 1$ ). Hence, we can conclude that, since this is the case, then, scaling up this pattern, i.e., if we only isolate a particular group of infected individuals without their potentially infected contacts, it would lead to have a group of infected individuals left inside the population to transmit the pathogen, where it is notable to refer that such cases act exponentially over the total



(a) Daily Infection Cases.



(b) Infectious Population Growth.

**Fig. 11** Epidemic spread in an uncontrolled environment and in an environment where is applied the countermeasure of density reduction (population capacity 50%)

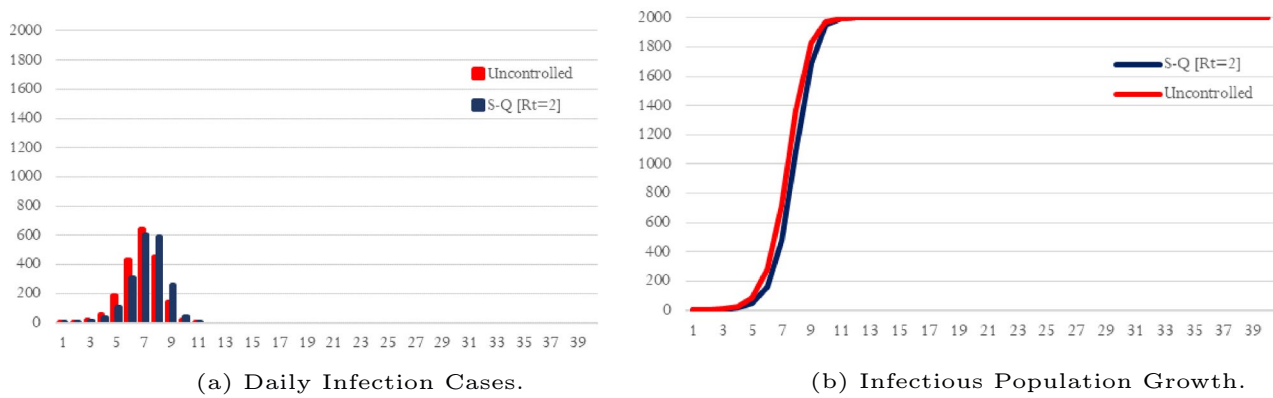


**Fig. 12** Epidemic spread in an uncontrolled environment and in an environment where is applied the countermeasure of self-quarantine without contact tracing

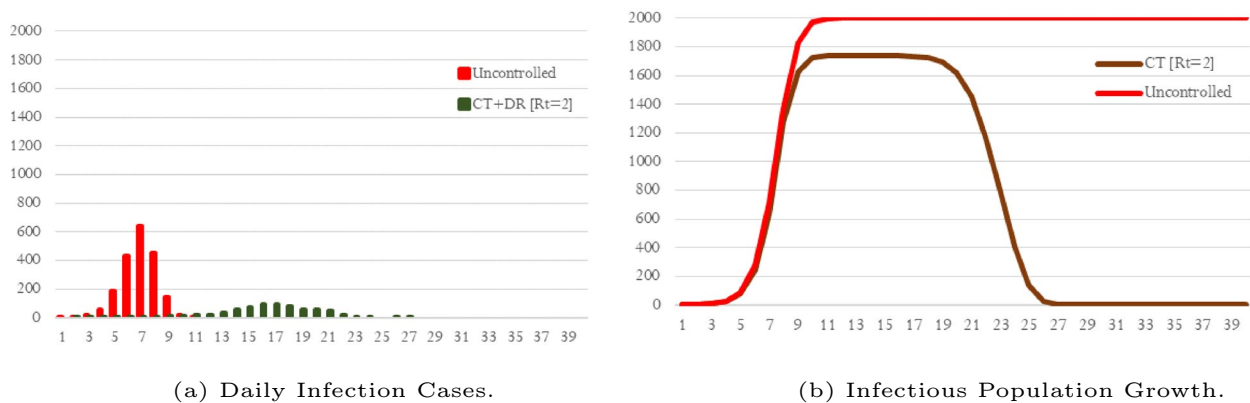


**Fig. 13** Epidemic spread in an uncontrolled environment and in an environment where is applied the countermeasure of self-quarantine with contact tracing

number of infected individuals across the time-line. Finally, an example could be considered the case of a “transmission tree”, where the sooner the contacts of a patient are isolated the less the tree-height will be, since the tree-height grows at most exponentially over each tree-level (in our case day of the experiment) across tree-height.

### 4.3.3 Contact tracing

Through this approach, we will examine the results after the deployment of a “spread aware application”, e.g., (Chondros et al. 2021), where in this series of experiments we assume that every infectious individual will be set to quarantine for 10 days, 2 days after symptoms, denoted as  $R_t = 2$ , referencing to the required response time for an individual that has been detected as infected to be set on quarantine. Considering the contact tracing procedure denoted by  $CT$  deployed by the smart application, the time an individual is detected as infected and set to quarantine, the most frequent contacts

of the last 2 days and the ones made the current day will all be informed via the application and they will also be set to quarantine for 10 days. As we can see from the exhibited results presented in Fig. 13a and b, the epidemic has been successfully mitigated in 26 days, with the reproduction number  $R_0$  starting from 1.3 at day 1, reaching a peak of 3.12 at day 5 and reduced below 1 from day 16 and later, leading to the decay of the epidemic by day 27, where most importantly, it is observed a significant reduction over the infectious population comparing the uncontrolled environment. More precisely, in Fig. 10b at day 11 in the experiment of the uncontrolled environment, all susceptible population have been infected resulting to a pandemic, where in contrast to the experiment after applying the countermeasure of the contact tracing the curve of the corresponding infectious individuals remains stable at almost 80% of the initial population until day 20. By day 21, in Fig. 13b, we observe a linear decreasing ratio of the curve until day 27 where the number of the infectious individuals has been eliminated,

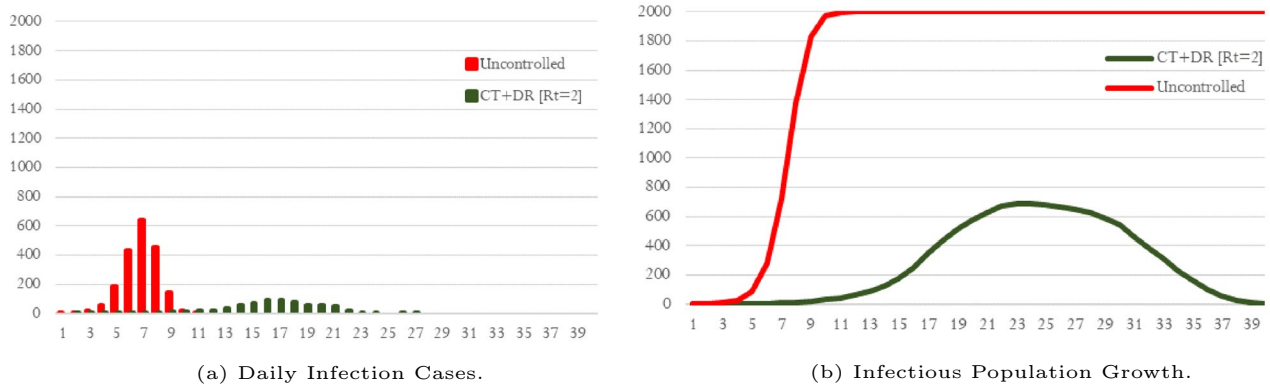


**Fig. 14** Epidemic spread in an uncontrolled environment and in an environment where are applied the countermeasures of density reduction and self-quarantine with contact tracing

with the pandemic, after the use of the deployment of this countermeasure, to be successfully prevented.

#### 4.3.4 Combination of counter measures

Next, we will discuss the results of our experiment after the application of the combination of countermeasures to mitigate the spread of the pathogen. The combined countermeasure we investigate, denoted by *CT + DR*, include the “density reduction” (denoted by *DR*) and the utilization of the spread aware application in “contact tracing” (denoted by *CT*) described previously. As we can see from the results presented in Fig. 14, we observe a Gaussian curve, where until day 10 the number of the infected population is retained very low, and from day 10 we observe an increase on the curve that reaches its top at day 25 with a ratio of 30% of infectious individuals over the initial susceptible population. The epidemic lasted 39 days until its elimination, exhibiting a reproduction number  $R_0$  starting from 1 at day 1, reaching a peak of 1.63 at day 11 and reduced below 1 by day

23 leading to the decay of the epidemic and consequently to pandemic prevention. By day 25 the curve decreases reaching to 0 infectious individuals, where at the end of the experiment the airborne pathogen has been eliminated since the individuals in the infectious state have been transformed to immune during quarantine or the ones that had not been infected remained susceptible, and the pandemic has been successfully prevented.

#### 4.3.5 Deploying the 2D-Co-contact algorithm

In Fig. 15, we illustrate the averaged results achieved over a series of experiments utilizing the proposed integrated simulation framework and deploying the Spread Awareness application with Contact Tracing utilizing the 2D-Co-Contact Algorithm and Density Reduction. As we can observe through the obtained results, denoted by 2DCC, there is exhibited a successful mitigation of the epidemic, where a very small portion of the susceptible population were infected by the pathogen. As we can observe from the

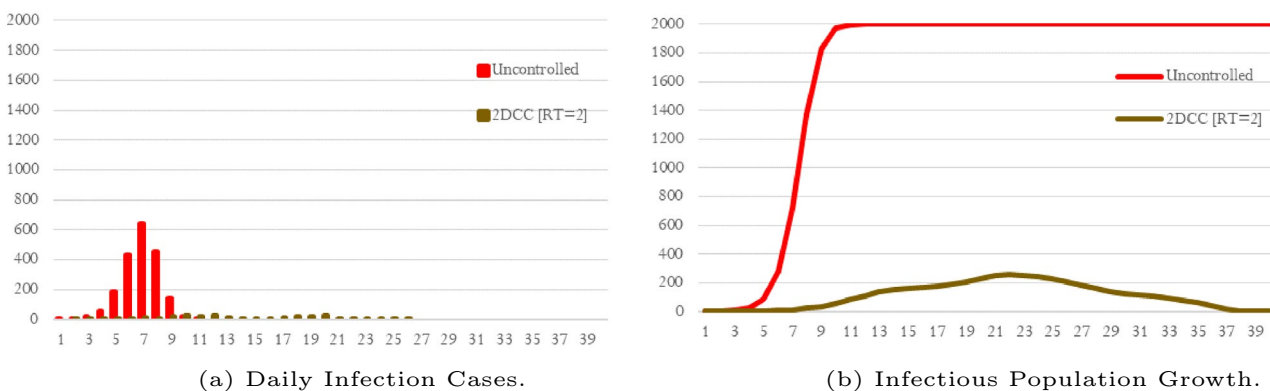


**Fig. 15** Epidemic spread in an uncontrolled environment and in an environment where are applied the countermeasures of density reduction and self-quarantine with contact tracing utilizing the 2D-Co-Contact Algorithm

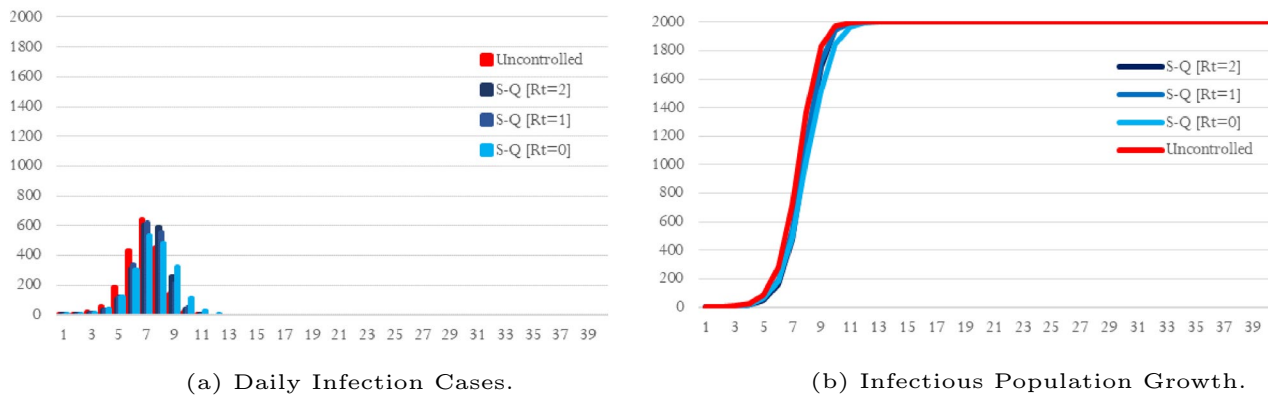


**Fig. 16** Epidemic spread in an uncontrolled environment and in an environment where is applied the countermeasure of self-quarantine without contact tracing for various response time values (i.e.,  $R_t = 2$ ,  $R_t = 1$ , and  $R_t = 0$ )

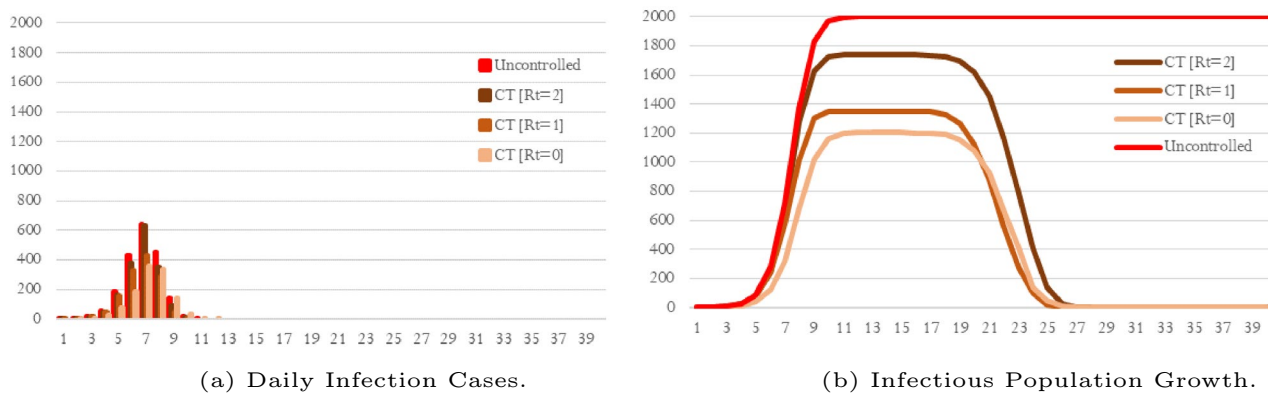


**Fig. 17** Epidemic spread in an uncontrolled environment and in an environment where is applied the countermeasure of self-quarantine with contact tracing for various response time values (i.e.,  $R_t = 2$ ,  $R_t = 1$ , and  $R_t = 0$ )

exhibited results presented in Fig. 15, the epidemic lasted 39 days exhibiting a reproduction number  $R_0$  starting from 1 at day 1, reaching a peak of 1.63 at day 5 and reduced below 1 by day 22 leading to the decay of the epidemic and consequently to pandemic prevention. Comparing the results of Fig. 15 to the ones achieved by the combined counter measure of “density reduction” and “contact tracing” without the utilization of the 2D-Co-Contact Algorithm (denoted by  $CT + DR$ ), as they are presented in Fig. 14, it is quite notable the reduction resulted to both the daily infection cases and to the maximum cumulative number of infectious population, where in particular for this case there is exhibited a reduction of 62% for day 22 and 63.15% for day 23 in the maximum number of infectious population compared to the results depicted in Fig. 14 by deploying solely the combination of “density reduction” and “contact tracing” countermeasures without the application of the 2D-Co-Contact Algorithm, where an average of 256 against 674 infectious individuals

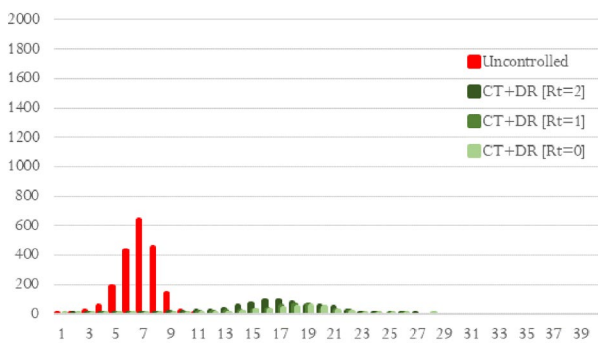
are exhibited in day 22, and 254 against 689.3 for day 23. More precisely, a reduction ranging from 62% for day 22 to 76.5% for day 30 is exhibited, where in particular for day 24, only a 12.3% of the total susceptible population have been infected by the airborne pathogen if the 2D-Co-Contact Algorithm is applied.

#### 4.3.6 Early warning by the decrease of response time

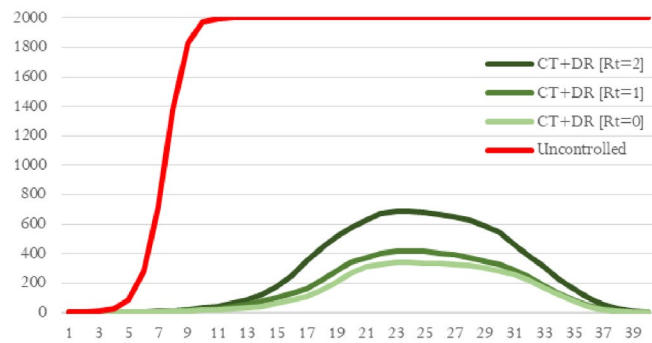
Next, we discuss the exhibited results over another series of experiments regarding the effect of “early warning” to pandemic prevention, i.e., the time required for an individual after symptoms onset to be set to quarantine and start if applicable the contact tracing procedure. Throughout this series of experiments, we examine the curve depicting the daily infection cases and the corresponding behavior of the infectious population growth curve by decreasing the response time  $R_t$ . Considering

the previous experiments that we assumed the “response time” was 2 days, i.e.,  $R_t = 2$ , we decrease the response time to  $R_t = 1$  and  $R_t = 0$  days, i.e., the infectious individual will be set to quarantine 1 day or the same day of the symptoms onset, respectively. In Fig. 16, we compare the results of the curves decreasing the response time to 1 and 0 days, denoted as  $S - Q[R_t = 2]$  for the reference case (“self-isolation”), and  $S - Q[R_t = 1]$  and  $S - Q[R_t = 0]$  for the cases under consideration, respectively. As we can observe from the exhibited results presented in Fig. 16, regardless the decrease in the response time  $R_t$ , in any case the pandemic could not be prevented, where for the case of  $R_t = 1$ , the epidemic evolved to pandemic in 12 days with the exhibited reproduction number  $R_0$  starting from 2.66 at day 1, reaching a peak of 3.7 at day 3, and for the case of  $R_t = 0$  the epidemic evolved to pandemic in 13 days with the exhibited reproduction number  $R_0$  starting from 2.3 at day 1, reaching a peak of 3.27 at day 4. Considering the daily infection cases depicted in Fig. 16a, we observe a Gaussian distribution in all cases and a similar number

of daily infection cases in  $R_t = 1$  and  $R_t = 2$  experiments. The bar plot of experiment with  $R_t = 0$ , compared to the ones exhibited by  $R_t = 1$  and  $R_t = 2$ , achieves a decreased maximum number of daily infection cases. As we can see from the results presented in Fig. 16b, a slight difference between the slopes of the infectious population growth curves is exhibited at day 8. As long as the response time is reduced, the corresponding slope of the curve shifts to the right, which imprints a slightly decreasing rate of the corresponding infectious population growth curve. The behavior of the corresponding curves and the similarity among them is affected mostly by the small number of infectious individuals that have been set to quarantine by the time the virus has been spread into the majority of the population. The number of infectious individuals that have been set to quarantine which reduces slightly the density of the city alongside the day that they were set to quarantine and the percentage of the infected population is not efficient. The corresponding results among these specific experiments are pairwise similar and the overall

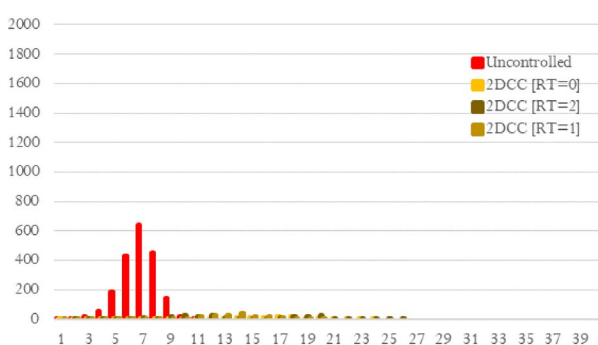


(a) Daily Infection Cases.

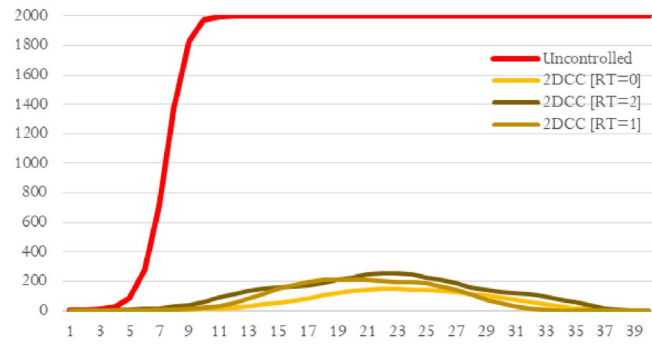


(b) Infectious Population Growth.

**Fig. 18** Epidemic spread in an uncontrolled environment and in an environment where are applied the countermeasures of density reduction and self-quarantine with contact tracing for various response time values (i.e.,  $R_t = 2$ ,  $R_t = 1$ , and  $R_t = 0$ )



(a) Daily Infection Cases.



(b) Infectious Population Growth.

**Fig. 19** Epidemic spread in an uncontrolled environment and in an environment where are applied the countermeasures of density reduction and self-quarantine with contact tracing utilizing the 2D-Co-Contact Algorithm for various response time values (i.e.,  $R_t = 2$ ,  $R_t = 1$ , and  $R_t = 0$ )

improvements over those results are not significant, since all individuals got infected as long as the prevention of the pandemic failed in all cases.

Next, we will discuss the exhibited results of the experiments presented in Fig. 17 after deploying the countermeasure of “contact tracing”, investigating the effect of response time in the “contact tracing” procedure and to a further extent to the mitigation of the epidemic. In Fig. 17a and b, we compare the results of the curves decreasing the response time the infected individual will be set to quarantine to 1 and 0 days after symptoms onset, alongside its contacts of the last two days, denoted as  $CT[Rt = 2]$  for the reference case, and  $CT[Rt = 1]$  and  $CT[Rt = 0]$ , respectively, for the cases under consideration. As we can observe in both cases presented in Fig. 17, i.e.,  $CT[Rt = 1]$  and  $CT[Rt = 0]$ , the epidemic has been successfully prevented before evolving to pandemic. Moreover, as we can observe from the exhibited results presented in Fig. 17a for  $Rt = 1$  the epidemic was mitigated in 27 days with the exhibited reproduction number  $R_0$  starting from 1.5 at day 1, reaching a peak of 3.15 at day 5 and reducing below 1 after day 14, while for the case of  $Rt = 0$ , the epidemic was mitigated in 26 days with the exhibited reproduction number  $R_0$  starting from 1 at day 1, reaching a peak of 3.13 at day 4 and reducing below 1 after day 14, leading in both cases to the decay of the epidemic and consequently to pandemic prevention. In particular, as we can observe through the curves presented in in Fig. 17b, at days 5 – 8, we observe an exponential increase of the infectious population growth, where the more the response time, the earlier the growth level starts and the higher the peak and the duration of the corresponding curve. Accordingly, the curve of the infectious population growth drops after day 22 considering its corresponding response time until the end of the experiment, which the number of infectious populations has been eliminated. In all the cases of response time under consideration, after at most 27 days, the countermeasure of “contact tracing” efficiently prevents the spread of the airborne pathogen.

In Fig. 18 we can see the curves after the application of the combination of the “density reduction” and “contact tracing” countermeasures, denoted by  $CT + DR$ , as response time  $Rt$  is reduced. Similarly to the previous experiments, regarding the effect of response time in pandemic mitigation, we investigate the effect of response time in the same cases, where in Fig. 18a and b, we compare the results of the curves decreasing the response time to 1 and 0, denoted as  $CT + DR[Rt = 2]$  for the reference case, and  $CT + DR[Rt = 1]$  and  $CT + DR[Rt = 0]$ , respectively, for the cases under consideration. As we can observe in both cases presented in Fig. 18, i.e.  $CT + DR[Rt = 1]$  and  $CT + DR[Rt = 0]$ , the epidemic has been successfully prevented before evolving to pandemic. Moreover, as we can see from the exhibited results presented in Fig. 18a for  $Rt = 1$  the epidemic suppressed in

26 days with the exhibited reproduction number  $R_0$  starting from 1 at day 1, reaching a peak of 2.25 at day 4 and reducing below 1 after day 24, while for the case of  $Rt = 0$ , the epidemic suppressed in 28 days with the exhibited reproduction number  $R_0$  starting from 1.33 at day 1, reaching a peak of 1.94 at day 7 and reducing below 1 after day 23, leading in both cases to the decay of the epidemic and consequently to pandemic prevention. We also observe that as response time increases, the grow level of the corresponding curve is increasing more aggressively and as we can see in the corresponding bar plots (see Fig. 18a) depicting the daily infection cases, the maximum daily infection cases decreases as the response time goes down and the Gaussian curve shifts right, delaying the spread of the pathogen. At the cumulative infectious population growth curve depicted in Fig. 18b, we observe a Gaussian distribution in all cases, whereas in the previous series of experiments, the more the response time, the earlier the start of the grow level of the curve. The peak of the curves is also decreasing as long as the response time decreases, where as we can see from the results depicted in Fig. 18b, the peak of the curve with  $Rt = 2$  is approximately at 35% of the initial population and for  $Rt = 0$  the corresponding peak of the curve does not exceed 17%, which lead us to infer that such a remarkable difference on the behavior of the curve setting different values of the response time makes the “early warning” a crucial factor for pandemic prevention.

Finally, observing Fig. 19, we can see that a further improvement can be achieved in the results by the deployment of the countermeasure of 2D-Co-Contact Algorithm, denoted by  $2DCC$ , when reducing the response time  $Rt$  to 1 and 0, denoted by  $2DCC[Rt = 1]$  and  $2DCC[Rt = 0]$  respectively, compared to the results of Fig. 15. As we can observe from both cases presented in Fig. 19, i.e.,  $2DCC[Rt = 1]$  and  $2DCC[Rt = 0]$ , the epidemic has been successfully prevented before evolving to pandemic. Moreover, as we can see from the exhibited results presented in Fig. 19 for  $Rt = 1$  the epidemic suppressed successfully with the exhibited reproduction number  $R_0$  starting from 1 at day 1, reaching a peak of 1.83 at day 3 and reducing below 1 after day 17, while for the case of  $Rt = 0$ , the epidemic was also suppressed with the exhibited reproduction number  $R_0$  starting from 1 at day 1, reaching a peak of 1.53 at day 7 and reducing below 1 after day 23, leading in both cases to the decay of the epidemic and consequently to pandemic prevention. The application of the 2D-Co-Contact Algorithm already augmented the combination of countermeasures of “contact tracing” and “density reduction” for  $Rt = 2$  in Fig. 18, while, a further decrease in the response time, i.e., for  $Rt = 1$ , and  $Rt = 0$ , the deployment of the 2D-Co-Contact Algorithm for  $Rt = 0$  augments the mitigation of the epidemic and even before it evolves to pandemic, there are even less daily infection

cases exhibited, as also the maximum cumulative number of infectious population is decrease over 50% compared to the so far optimal approach of deploying solely the countermeasures of “contact tracing” and “density reduction” with  $R_t = 0$ .

## 5 Conclusion

In this section, we conclude our work regarding the development of the integrated simulation framework and the experimental study conducted utilizing the proposed framework focusing on pandemic prevention and mitigation in the area of airborne diseases, setting also our aims for further research.

### 5.1 Discussion over the exhibited results

Next, we provide an analysis over the behavior of the propagation of the airborne pathogen with respect to the properties of SARS-CoV-2 that were taken into account over our simulation experiments in the corresponding propagation model in an environment that no countermeasure is applied, while we discuss to a further extent the effectiveness of the deployed countermeasures and compare them utilizing, among other criteria, the estimations on potential deaths caused by the pathogen.

#### 5.1.1 Behavioral analysis of epidemic

Throughout the behavioral analysis of the epidemic spread, we will discuss the exhibited results and the behavior of the pathogen spread after applying the countermeasures that we mentioned before to prevent the pandemic. In an uncontrolled environment, the spread of the pathogen is aggressive and infects all the initially susceptible population until day 10. The same results were exhibited after the quarantine of the individuals (without setting to quarantine their contacts) since was not enough to limit the spread of the pathogen and prevent the pandemic. Applying the “density reduction” countermeasure, in the corresponding series of experiments we observed an approximately 12-day delay of the pandemic of the initial population. The number of the infected individuals over the days was decreased and the spread of the airborne pathogen was slower compared the one exhibited in an uncontrolled environment. However, this countermeasure was not enough to prevent the pandemic.

On the other hand, the deployment of “contact tracing” procedure was the first countermeasure that performed effectively to prevent the pandemic. At the first 7 days, the corresponding infectious population growth curve is similar to the curve of the spread in an uncontrolled environment since no countermeasure has been applied. In the first day

of the activation of the quarantine of the infectious individuals (after the symptoms onset in the initial infected population) alongside their corresponding contacts, we observed a huge decrease of the daily infection cases and a stabilization on the overall infected population. The quarantine measure decreased the density of the population in the area of the city which slowed down the spread of the pathogen and protected an adequate portion of the susceptible individuals after setting them to quarantine (i.e., a portion of contacts of an infectious individuals been set to quarantine were still susceptible but not infected). This countermeasure performed effectively enough to slow down the spread of the pathogen, leaving a period of time for the infectious individuals to cure, becoming immune and prevent the pandemic.

Next, the countermeasure that deployed the incorporation of both “density reduction” and “contact tracing” countermeasures, slowed down the spread of the pathogen at the very first days and prevented the pandemic due to the immediate reduction of the population moving in the area of the city and kept the daily infection cases at low levels after setting the infected individuals alongside their corresponding contacts to quarantine throughout the “contact tracing” procedure deployed. Finally, the augment of the “contact tracing” procedure incorporating the 2D-Co-Contact Algorithm when deployed over the combination of “density reduction” and “contact tracing” countermeasures, especially for the case where the response time is minimized, i.e.,  $R_t = 0$ , exhibited the optimal results being the most effective combination of countermeasures. The proposed approach achieved a minimum of infectious population in the cumulative curve ensuring that a very low portion of the susceptible population were infected by the virus, eliminating the overall risks that potentially may be caused by the pathogen as we will discuss later, while also mitigated and prevented the pandemic more effectively than the any other countermeasure.

#### 5.1.2 Effectiveness of the proposed approaches

Next, we discuss the effectiveness of the proposed countermeasures in preventing and mitigating the pandemic, as it is shown throughout the exhibited experimental simulation results regarding four factors, namely, the overall control of the epidemic, the maximum infection cases exhibited, the duration the epidemic lasted, and the number of potential deaths avoided by the deployment of each countermeasures.

**5.1.2.1 Epidemic control** Considering the analysis of the pandemic over an uncontrolled environment and after the application of the most effective countermeasures investigated, the spread in an uncontrolled environment seems to evolves rapidly and the pandemic after a few days is unavoidable. The countermeasure of the “density reduction” at first days seems to be efficient since the number of daily

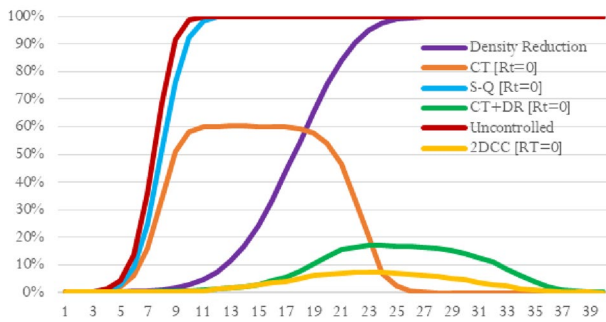


**Fig. 20** Comparative results among all the proposed countermeasures

infection cases is retained at low levels. However, across the days of the epidemic evolution, the infection cases were increasing until all the population got infected, resulting to a pandemic.

The first countermeasure that successfully prevented the pandemic was the deployment of “contact tracing” procedure, which is able to track the contacts of individuals that have been detected as infected. Until the early stages of the epidemic, where the first infected individual is set to quarantine, i.e., the first infection case that will enable the countermeasure, the spread of the pathogen behaves similarly as in the case of an uncontrolled environment, where through the days after the activation of the countermeasure the epidemic starts to decay. However, despite the effectiveness of this countermeasure in pandemic prevention, over the half portion of the susceptible population had not avoided the infection by the spreading airborne pathogen.

The incorporation of both “density reduction” and “contact tracing” countermeasures into a common countermeasure was one of the most efficient countermeasures since the number of the daily infection cases was retained at low levels and the majority of the population avoided to get infected until the pandemic prevention. Throughout this approach, a further improvement regarding the “contact tracing” countermeasure its augment by the application of the 2D-Co-Contact Algorithm performed even more effectively, preventing the susceptible population by allowing even less daily infection cases resulting to a lower maximum of infectious population and finally to a pandemic prevention.

**5.1.2.2 Maximum infection cases** Regarding the maximization of the overall infection cases, in Fig. 20, we observe a similar behavior among the experiments in an uncontrolled environment, and the ones with the deployment the countermeasures of “density reduction” and “self-isolation”, since they reach their corresponding peaks at days 9 and 27, 11, respectively. On the other hand, the experiments with the combination of the countermeasures of “contact tracing” and “density reduction” perform better since they appear

their corresponding peak at day 24 with approximately 380 cases (instead of 1200 for the previous cases).

Additionally, for the series of experiments regarding the cases of the spread in an uncontrolled environment, the countermeasure of “self-isolation” and the countermeasure of “contact tracing”, in Fig. 20, we observe an early increase from day 5 in all the cases of experiments. This behavior is attributed to the fact the no “density reduction” is applied in the susceptible population of the area in any experiment case; whereas for the case of the deployment of the “contact tracing” countermeasure, the behavior is differentiated later since it lasts an average of 7 days for an infected individual to reach the symptoms onset enabling thus the procedure of setting to quarantine this individual alongside its recent contacts, that consequently yields later a control of the epidemic by stabilizing the infectious population from days 11 to 17.

On the other hand, incorporating both the “contact tracing” and the “density reduction” countermeasures, alongside a minimization of the response time, the grow level appears approximately at day 15 since the “density reduction” countermeasure delays the epidemic growth resulting to a better performance compared to the previous counter measure (i.e., “contact tracing” without “density reduction”) for the same response time that exhibited the grow level at day 5. Moreover, the further improvement of this approach by the augment of the “contact tracing” procedure with the deployment of the 2D-Co-Contact Algorithm achieved also a pandemic prevention by eliminating the epidemic even earlier, having additionally a less maximum number of infectious population for the case where the response time is minimized, compared to the case of the combination of countermeasures of “contact tracing” and “density reduction” without the application of 2D-Co-Contact Algorithm for the contact tracing procedure.

**5.1.2.3 Duration of the epidemic** In the discussion of the exhibited results, we examine both the duration of the epidemic alongside the maximum daily infection cases under the aspect of a countermeasure to successfully prevent a pandemic. However, to this point, it is important to note that the overall duration of the pandemic should not consist a strict criterion on the effectiveness of a countermeasure in pandemic prevention since an effective countermeasure may exhibit a longer period until the elimination of the epidemic but to exhibit also a very low number of daily infection cases.

Concerning the duration of the high levels, considering Fig. 20, the experiment in an uncontrolled environment, the “density reduction” and the “self-quarantine” countermeasures since they result to a pandemic, they perform the worst. The “contact tracing” countermeasure retains its corresponding duration in high levels for 8 days compared the combination of “contact tracing” and “density reduction”

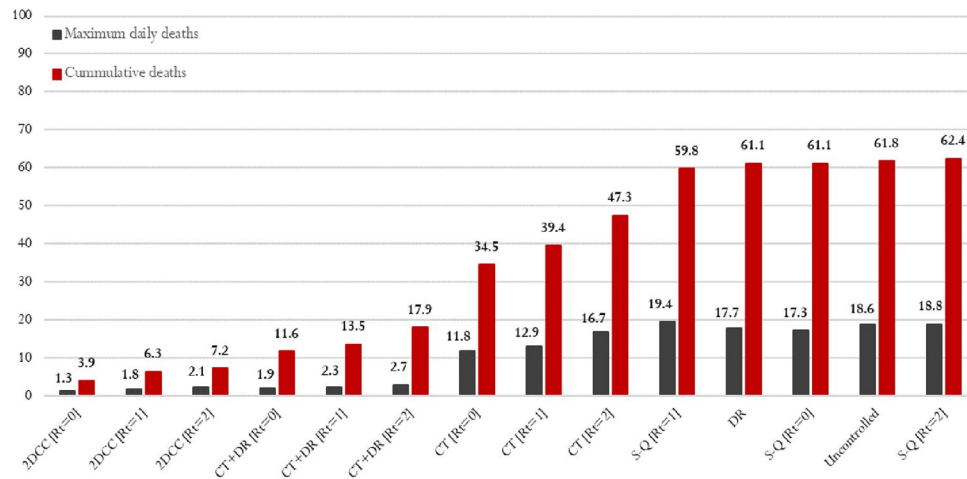


**Fig. 21** Global estimation of potential deaths by the daily confirmed cases of each experiment

countermeasures which their duration lasted less than 5 days, while the optimal results are achieved from the deployment of the 2D-Co-Contact Algorithm over the combination of ‘contact tracing’ and ‘density reduction’ countermeasures, resulting to a 3-day peak duration being the most effective countermeasure that achieves a pandemic prevention with the least peak duration.

Additionally, observing the overall duration of the epidemic, the experiments with uncontrolled environment and ‘self-quarantine’ perform the worst since they both reach the pandemic at day 11. The ‘density reduction’ countermeasure delays but does not prevent the pandemic since approximately at day 24 all the susceptible individuals have been infected. At last, the countermeasure that combines both the ‘density reduction’ and the ‘contact tracing’ countermeasures needs 37 days to eliminate the pandemic unlike the counter measure of ‘contact tracing’, which eliminates the pandemic at 26 days but having an almost three times more the size of infected individuals.

Finally, the deployment of the 2D-Co-Contact Algorithm over the combination of ‘density reduction’ and ‘contact tracing’ countermeasures exhibited the optimal performance among the rest of the countermeasures, allowing the less infections among the susceptible population and not only performed better than the countermeasure that combined the ‘density reduction’ and the ‘contact tracing’ in terms of maximum infection cases, but also achieved a more earlier elimination of the epidemic.

**5.1.2.4 Potential death cases avoided** Finally, another interesting observation, with respect to the death case rates, based on analysis data regarding the mortality rate of SARS-CoV-2 (Johns Hopkins University of Medicine 2020) that set this rate to almost 0.3%, we computed the estimated

averaged numbers of potential death cases considering the daily infection cases over our previous mentioned experiments. In Fig. 21, we present the averaged estimated numbers (y-axis) regarding the maximum daily potential deaths (gray color) and the cumulative potential deaths (red color), for all the deployed approaches (x-axis). The averaged rates of potential deaths regarding the daily infection cases and the cumulative deaths refer to the number of infected individuals that fall in the rate of 0.3% of not surviving.

As we can observe, the cumulative daily deaths are similar comparing the experiments which result to a pandemic, i.e., uncontrolled environment, ‘self-isolation’ in all the response times, and ‘density reduction’. However, the maximum daily death cases vary among the mentioned experiments since they slightly decrease as long as the response time decreases. It is important to note that the number of cumulative deaths appears to be irrelevant to the delay of the pandemic as long as the prevention has been failed. The countermeasure that exhibited an adequate performance concerning the number of cumulative and maximum daily death cases are the combination of ‘contact tracing’ and ‘density reduction’, i.e., CT+DR which decreased the corresponding number of death cases as the response time decreases. Moreover, it is important to refer the difference of the results among CT+DR[ $R_t = 0$ ] and CT+DR[ $R_t = 2$ ], where the minimization of response time results to an approximate of 40% decrease over the corresponding cumulative death cases, depicting, thus, the crucial importance of this factor.

Finally, the optimally performed countermeasure that incorporated the utilization of 2D-Co-Contact Algorithm over the combination of ‘contact tracing’ and ‘density reduction’ countermeasures augmenting the contact tracing procedure, exhibited the minimum death cases so in the case of cumulative death cases as in the case of maximum

daily death cases exhibited, achieving almost an elimination on the average number of maximum daily death cases for  $R_t = 0$ , performing similarly for  $R_t = 1$  and  $R_t = 2$ , while the cumulative potential death cases in the maximum response time, i.e.,  $R_t = 2$  was almost 7 individuals compared to the 11 individuals that potentially would not survive if the 2D-Co-Contact Algorithm would not be applied ( $CT + DR$  [ $R_t = 0$ ]) and even better compared to the case where no countermeasure is deployed, achieving, hence, the avoidance of almost 60 deaths.

## 5.2 Concluding remarks

In this work, we examined the behavior and the evolution of the spread of an airborne pathogen in an uncontrolled environment of a city and established a set of countermeasures to prevent an epidemic to evolve to pandemic using our proposed integrated simulation framework for the pandemic mitigation and prevention. We conducted an experimental study over a series of simulation experiments to evaluate the effect of various countermeasures in the mitigation of the spread of an airborne pathogen taking into account the properties of SARS-CoV-2, proposing, finally an algorithm that proactively augments the contact tracing procedure that experimentally proved its potentials to mitigate and eliminate the spread of an airborne disease. Regarding the proposed integrated simulation framework for the pandemic prevention and mitigation, we designed and implemented three sub-models, namely the spatial, the mobility, and the propagation models, to be incorporated for the integration of the simulation framework. We implemented those models incorporated by the proposed integrated simulation framework and performed a series of sequential experiments to examine the spread dynamics in an uncontrolled environment and the impact provided by the application of a set of countermeasures considering different values of the response time. Finally, we presented and discussed extensively the application of each countermeasure, namely “density reduction”, “self-quarantine”, “contact tracing”, combinations of them, the design of the 2D-Co-Contact Algorithm that proactively augments the contact tracing procedure, deployed for pandemic mitigation and prevention. Finally, we discussed the exhibited experimental results, the impact of each specific countermeasure and the effect of response time in pandemic prevention concluding into an ordering regarding the effectiveness of each countermeasure with respect in both the characteristics depicted by the behavior of the curve that represent the infected population, as also the estimated numbers of potentials death cases caused by the pathogen that may occur among the infected individuals.

## 5.3 Future research

Throughout our research, we concluded that the procedure of contact tracing through the utilization of efficient techniques is a determining and of major importance factor for limiting the spread of an aggressively transmitted airborne pathogen, like in our case the SARS-CoV-2, and preventing a pandemic, especially considering also the importance of the effect of early warning in terms of low response time, which reduces both the daily and the total number of infection cases. Considering the results achieved through our experimental study and the information explored across this work, we focus to extend our research, besides optimizing our current platform, by implementing a variety of functions that can dynamically navigate a individual to a destination point in a city avoiding congested areas, and monitoring in real-time the infection risk of particular city areas considering the traces of individuals related to infected contacts. Finally, an extensive study and research is required to ensure the efficacy and the effectiveness of the resulting techniques, regarding the underlying simulation framework and the corresponding countermeasures, to cover cases beyond the airborne pathogens that may arise in the future.

**Funding** Not applicable

**Availability of data and materials** Not applicable

**Code availability** The code of the integrated simulation framework for the prevention and mitigation of pandemics caused by airborne pathogens proposed in this work is available from Github in the repository named AlgoLab under folder Epidemics (<https://github.com/AlgoLabUOI/AlgoLab/tree/main/epidemics>).

## Declarations

**Conflict of interests** Not applicable.

**Ethics approval** Not applicable.

**Consent to participate** Not applicable.

**Consent for publication** Not applicable.

## References

- Achaiah NC, Subbarajasetty SB, Shetty RM (2020) R0 and re of covid- 19: can we predict when the pandemic outbreak will be contained? Indian J Crit Care Med Peer Rev Offl Publ Indian Soc Crit Care Med 24(11):1125. <https://doi.org/10.5005/jp-journals-10071-23649>
- Akinbi A, Forshaw M, Blinkhorn V (2021) Contact tracing apps for the covid-19 pandemic: a systematic literature review of challenges and future directions for neo-liberal societies. Health Inf Sci Syst 9(1):1–15. <https://doi.org/10.1007/s13755-021-00147-7>

- Algorithms Engineering Laboratory (2022) Algotlab/epi-demics at main algolabuoi/algolab. <https://github.com/AlgoLabUOI/AlgoLab/tree/main/epidemics>
- Anand S, Mayya Y (2020) Size distribution of virus laden droplets from expiratory ejecta of infected subjects. *Sci Rep* 10(1):1–9. <https://doi.org/10.1038/s41598-020-78110-x>
- Bahl P, Doolan C, de Silva C, Chughtai AA, Bourouiba L, MacIntyre CR (2020) Airborne or droplet precautions for health workers treating coronavirus disease 2019? *J Infect Dis*. <https://doi.org/10.1093/infdis/jiaa189>
- Barmak DH, Dorso CO, Otero M (2016) Modelling dengue epidemic spreading with human mobility. *Physica A* 447:129–140. <https://doi.org/10.1016/j.physa.2015.12.015>
- Becker AD, Grenfell BT (2017) tsir: an r package for time-series susceptible-infected-recovered models of epidemics. *PLoS ONE* 12(9):e0185528. <https://doi.org/10.1371/journal.pone.0185528>
- Bertacchini F, Bilotta E, Pantano PS (2020) On the temporal spreading of the sars-cov-2. *PLoS ONE* 15(10):e0240777. <https://doi.org/10.1371/journal.pone.0240777>
- Britton T (2010) Stochastic epidemic models: a survey. *Math Biosci* 225(1):24–35. <https://doi.org/10.1016/j.mbs.2010.01.006>
- Center for Disease Control and Prevention (2020). Interim clinical guidance for management of patients with confirmed coronavirus disease (COVID-19) (Tech. Rep.)
- Chondros C, Georgiou-Mousses C, Nikolopoulos SD, Polenakis I, Vouronikos V (2021) Sarissa-a mobile application for the proactive control of sars-cov-2 spread. *arXiv preprint arXiv:2106.14567*. <https://doi.org/10.48550/arXiv.2106.14567>
- Chondros C, Nikolopoulos SD, Polenakis I (2021) A stochastic graph-based model for the simulation of sars-cov-2 transmission. *arXiv preprint arXiv:2111.05802*. <https://doi.org/10.48550/arXiv.2111.05802>
- Cirincione L, Plescia F, Ledda C, Rapisarda V, Martorana D, Moldovan RE, Cannizzaro E (2020) Covid-19 pandemic: prevention and protection measures to be adopted at the workplace. *Sustainability* 12(9):3603. <https://doi.org/10.3390/su12093603>
- Cliff OM, Harding N, Piraveenan M, Erten EY, Gambhir M, Prokopenko M (2018) Investigating spatiotemporal dynamics and synchrony of in uenza epidemics in Australia: an agent-based modeling approach. *Simul Model Pract Theory* 87:412–431. <https://doi.org/10.1016/j.simpat.2018.07.005>
- Cortellessa G, Stabile L, Arpino F, Faleiros DE, Bos Wvd, Morawska L, Buonanno G (2021) Close contact risk assessment for sars-cov-2 infection. *arXiv preprint arXiv:2104.10934*. <https://doi.org/10.48550/arXiv.2104.10934>
- Cuevas-Maraver J, Kevrekidis PG, Chen Q-Y, Kevrekidis GA, Villalobos-Daniel V, Rapti Z, Drossinos Y (2021) Lockdown measures and their impact on single-and two-age-structured epidemic model for the COVID-19 outbreak in mexico. *Math Biosci* 336:108590. <https://doi.org/10.1016/j.mbs.2021.108590>
- Currie CS, Fowler JW, Kotiadis K, Monks T, Onggo BS, Robertson DA, Tako AA (2020) How simulation modelling can help reduce the impact of COVID-19. *J Simul* 14(2):83–97. <https://doi.org/10.1080/17477778.2020.1751570>
- Dhand R, Li J (2020) Coughs and sneezes: their role in transmission of respiratory viral infections, including sars-cov-2. *Am J Respir Crit Care Med* 202(5):651–659. <https://doi.org/10.1164/rccm.202004-1263PP>
- Dijkstra EW (1959) A note on two problems in connexion with graphs. *Numerische Mathematik* 1(1):269–271. <https://doi.org/10.1145/3544585.3544600>
- Drossinos Y, Stilianakis NI (2020) What aerosol physics tells us about airborne pathogen transmission. *Aerosol Sci Technol* 54(6):639–643. <https://doi.org/10.1080/02786826.2020.1751055>
- Duan W, Fan Z, Zhang P, Guo G, Qiu X (2015) Mathematical and computational approaches to epidemic modeling: a comprehensive review. *Front Comp Sci* 9(5):806–826. <https://doi.org/10.1007/s11704-014-3369-2>
- Hufnagel L, Brockmann D, Geisel T (2004) Forecast and control of epidemics in a globalized world. *Proc Natl Acad Sci* 101(42):15124–15129. <https://doi.org/10.1073/pnas.0308344101>
- Hughes JM, Wilson ME, Pike BL, Saylor KE, Fair JN, LeBreton M, Wolfe ND (2010) The origin and prevention of pandemics. *Clin Infect Dis* 50(12):1636–1640. <https://doi.org/10.1086/652860>
- Johns Hopkins University of Medicine (2020). Mortality analyses (Technical documents)
- Jung E, Iwami S, Takeuchi Y, Jo T-C (2009) Optimal control strategy for prevention of avian influenza pandemic. *J Theor Biol* 260(2):220–229. <https://doi.org/10.1016/j.jtbi.2009.05.031>
- Karita HCS, Dong TQ, Johnston C, Neuzil KM, Paasche-Orlow MK, Kissinger PJ et al (2022) Trajectory of viral rna load among persons with incident sars-cov-2 g614 infection (wuhan strain) in association with covid-19 symptom onset and severity. *JAMA Netw Open* 5(1):e2142796–e2142796. <https://doi.org/10.1001/jamanetworkopen.2021.42796>
- Katre P, Banerjee S, Balusamy S, Sahu KC (2021) Fluid dynamics of respiratory droplets in the context of COVID-19: Airborne and surfaceborne transmissions. *Phys Fluids* 33(8):081302. <https://doi.org/10.1063/5.0063475>
- Keeling MJ, Eames KT (2005) Networks and epidemic models. *J R Soc Interface* 2(4):295–307. <https://doi.org/10.1098/rsif.2005.0051>
- Kevrekidis PG, Cuevas-Maraver J, Drossinos Y, Rapti Z, Kevrekidis GA (2021) Reaction-diffusion spatial modeling of COVID-19: Greece and Andalusia as case examples. *Phys Rev E* 104(2):024412. <https://doi.org/10.1103/PhysRevE.104.024412>
- Kovacevic R, Stilianakis NI, Veliov VM (2020) A distributed optimal control epidemiological model applied to COVID-19 pandemic. Available as ORCOS Research Report, 13
- Lippi G, Simundic A-M, Plebani M (2020) Potential preanalytical and analytical vulnerabilities in the laboratory diagnosis of coronavirus disease 2019 (COVID-19). *Clin Chem Lab Med (CCLM)* 58(7):1070–1076. <https://doi.org/10.1515/cclm-2020-0285>
- Liu Q-H, Xiong X, Zhang Q, Perra N (2018) Epidemic spreading on time-varying multiplex networks. *Phys Rev E* 98(6):062303. <https://doi.org/10.1103/PhysRevE.98.062303>
- Loh EH, Zambrana-Torrel C, Olival KJ, Bogich TL, Johnson CK, Mazet JA, Daszak P (2015) Targeting transmission pathways for emerging zoonotic disease surveillance and control. *Vector-Borne Zoonotic Dis* 15(7):432–437. <https://doi.org/10.1089/vbz.2013.1563>
- Manika D, Golden LL (2011) Self-efficacy, threat, knowledge and information receptivity: exploring pandemic prevention behaviors to enhance societal welfare. *Acad Health Care Manag J* 7(1):31
- Masuda N, Holme P (2013) Predicting and controlling infectious disease epidemics using temporal networks. *F1000Prime Rep*. <https://doi.org/10.12703/P5-6>
- Modi K, Umate L, Makade K, Dubey RS, Agarwal P (2021) Simulation based study for estimation of COVID-19 spread in India using Seir model. *J Interdiscip Math* 24(2):245–258. <https://doi.org/10.1080/09720502.2020.1838059>
- Morse SS, Mazet JA, Woolhouse M, Parrish CR, Carroll D, Karesh WB, Daszak P (2012) Prediction and prevention of the next pandemic zoonosis. *Lancet* 380(9857):1956–1965. [https://doi.org/10.1016/S0140-6736\(12\)61684-5](https://doi.org/10.1016/S0140-6736(12)61684-5)
- Nadini M, Sun K, Ubaldi E, Starnini M, Rizzo A, Perra N (2018) Epidemic spreading in modular time-varying networks. *Sci Rep* 8(1):1–11. <https://doi.org/10.1038/s41598-018-20908-x>
- Nicas M, Nazaroff WW, Hubbard A (2005) Toward understanding the risk of secondary airborne infection: emission of respirable pathogens. *J Occup Environ Hyg* 2(3):143–154. <https://doi.org/10.1080/15459620590918466>

- Nikolopoulos SD, Polenakis I (2016) A model for establishing response-time bounds to prevent malware pandemics in mobile devices. In: Proceedings of the 17th international conference on computer systems and technologies 2016 pp 97–104. <https://doi.org/10.1145/2983468.2983475>
- Nikolopoulos SD, Polenakis I (2017) Preventing malware pandemics in mobile devices by establishing response-time bounds. *J Inf Secur Appl* 37:1–14. <https://doi.org/10.1016/j.jisa.2017.09.002>
- Obadia T, Haneef R, Boëlle P-Y (2012) The r0 package: a toolbox to estimate reproduction numbers for epidemic outbreaks. *BMC Med Inform Decis Mak* 12(1):1–9. <https://doi.org/10.1186/1472-6947-12-147>
- Organization WH (2021) Considerations for quarantine of contacts of COVID-19 cases: interim guidance, 19 august 2020 (Technical documents)
- Seminara G, Carli B, Forni G, Fuzzi S, Mazzino A, Rinaldo A (2020) Biological uid dynamics of airborne COVID-19 infection. *Scienze fisiche e naturali Rendiconti Lincei*. <https://doi.org/10.1007/s12210-020-00938-2>
- Stawicki SP, Jeanmonod R, Miller AC, Paladino L, Gaieski DF, Yaffee AQ et al (2020) The 2019–2020 novel coronavirus (severe acute respiratory syndrome coronavirus 2) pandemic: A joint American college of academic international medicine-world academic council of emergency medicine multidisciplinary COVID-19 working group consensus paper. *J Glob Infect Dis* 12(2):47. [https://doi.org/10.4103/jgid.jgid\\_86\\_20](https://doi.org/10.4103/jgid.jgid_86_20)
- Stilianakis NI, Drossinos Y (2010) Dynamics of infectious disease transmission by inhalable respiratory droplets. *J R Soc Interface* 7(50):1355–1366. <https://doi.org/10.1098/rsif.2010.0026>
- Tizzani M, Lenti S, Ubaldi E, Vezzani A, Castellano C, Burioni R (2018) Epidemic spreading and aging in temporal networks with memory. *Phys Rev E* 98(6):062315. <https://doi.org/10.1103/PhysRevE.98.062315>
- Valdano E, Fiorentin MR, Poletto C, Colizza V (2018) Epidemic threshold in continuous-time evolving networks. *Phys Rev Lett* 120(6):068302. <https://doi.org/10.1103/PhysRevLett.120.068302>
- Wei J, Li Y (2016) Airborne spread of infectious agents in the indoor environment. *Am J Infect Control* 44(9):S102–S108. <https://doi.org/10.1016/j.ajic.2016.06.003>

**Publisher's Note** Springer Nature remains neutral with regard to jurisdictional claims in published maps and institutional affiliations.

Springer Nature or its licensor holds exclusive rights to this article under a publishing agreement with the author(s) or other rightsholder(s); author self-archiving of the accepted manuscript version of this article is solely governed by the terms of such publishing agreement and applicable law.